Theses and Dissertations   1. Thesis and Dissertation Collection, all items

2008-12

THz-imaging Through-the-Wall using the Born and Rytov approximation

Lee, Kwangmoon

Monterey California. Naval Postgraduate School

https://hdl.handle.net/10945/3739

NAVAL POSTGRADUATE SCHOOL

MONTEREY, CALIFORNIA

THESIS

THz-IMAGING THROUGH-THE-WALL USING THE
BORN AND RYTOV APPROXIMATION

by

Kwangmoon Lee

December 2008

Thesis Advisor:	Brett Borden
Second Reader:	Gamani Karunisiri

Approved for public release, distribution is unlimited.

THIS PAGE INTENTIONALLY LEFT BLANK

REPORT DOCUMENTATION PAGE		*Form Approved OMB No. 0704-0188*
Public reporting burden for this collection of information is estimated to average 1 hour per response, including the time for reviewing instruction, searching existing data sources, gathering and maintaining the data needed, and completing and reviewing the collection of information. Send comments regarding this burden estimate or any other aspect of this collection of information, including suggestions for reducing this burden, to Washington headquarters Services, Directorate for Information Operations and Reports, 1215 Jefferson Davis Highway, Suite 1204, Arlington, VA 22202-4302, and to the Office of Management and Budget, Paperwork Reduction Project (0704-0188) Washington DC 20503.		
1. AGENCY USE ONLY *(Leave blank)*	**2. REPORT DATE** December 2008	**3. REPORT TYPE AND DATES COVERED** Master's Thesis
4. TITLE AND SUBTITLE THz-Imaging Through-the-Wall using the Born and Rytov Approximation		**5. FUNDING NUMBERS**
6. AUTHOR(S) Kwangmoon Lee		
7. PERFORMING ORGANIZATION NAME(S) AND ADDRESS(ES) Naval Postgraduate School Monterey, CA 93943-5000		**8. PERFORMING ORGANIZATION REPORT NUMBER**
9. SPONSORING /MONITORING AGENCY NAME(S) AND ADDRESS(ES) N/A		**10. SPONSORING/MONITORING AGENCY REPORT NUMBER**
11. SUPPLEMENTARY NOTES The views expressed in this thesis are those of the author and do not reflect the official policy or position of the Department of Defense or the U.S. Government.		
12a. DISTRIBUTION / AVAILABILITY STATEMENT Approved for public release; distribution is unlimited.		**12b. DISTRIBUTION CODE**
13. ABSTRACT (maximum 200 words) We investigated an inverse imaging problem by applying the Rytov approximation for Through-the-Wall Imaging using THz waves. In the beginning, we studied some properties of THz waves and the physical conditions for THz imaging in matter. Then we started with Maxwell's equations to derive a model for the transmission of Green's functions and used a Lippman-Schwinger integral equation and Rytov approximation to predict the scattered field. We applied the L-curve method for the selection of regularization parameters and then presented the reconstruction algorithm and illustrated the result with numerical simulations. We also compare this result to the one obtained by the Born approximation.		
14. SUBJECT TERMS Terahertz, Imaging, Born/Rytov approximation, Singular Value Decomposition		**15. NUMBER OF PAGES** 101
		16. PRICE CODE
17. SECURITY CLASSIFICATION OF REPORT Unclassified	**18. SECURITY CLASSIFICATION OF THIS PAGE** Unclassified	**19. SECURITY CLASSIFICATION OF ABSTRACT** Unclassified	**20. LIMITATION OF ABSTRACT** UU

THIS PAGE INTENTIONALLY LEFT BLANK

**THz-IMAGING THROUGH-THE-WALL USING THE BORN
AND RYTOV APPROXIMATION**

Kwangmoon Lee
Lieutenant, Korea Navy
B.S., Mechanics., Korea Naval Academy, 1998

Submitted in partial fulfillment of the
requirements for the degree of

MASTER OF SCIENCE IN PHYSICS

from the

**NAVAL POSTGRADUATE SCHOOL
December 2008**

Author:　　　　　　　Kwangmoon Lee

Approved by:　　　　　Brett Borden
　　　　　　　　　　　Thesis Advisor

　　　　　　　　　　　Gamani Karunasiri
　　　　　　　　　　　Second Reader

　　　　　　　　　　　James Luscombe
　　　　　　　　　　　Chairman, Department of Physics

iii

THIS PAGE INTENTIONALLY LEFT BLANK

ABSTRACT

We investigated an inverse imaging problem by applying the Rytov approximation for Through-the-Wall Imaging using THz waves. In the beginning, we studied some properties of THz waves and the physical conditions for THz imaging in matter. Then we started with Maxwell's equations to derive a model for the transmission of Green's functions and used a Lippman-Schwinger integral equation and Rytov approximation to predict the scattered field. We applied the L-curve method for the selection of regularization parameters, and then presented the reconstruction algorithm and illustrated the result with numerical simulations. We also compared this result to the one obtained by the Born approximation.

THIS PAGE INTENTIONALLY LEFT BLANK

TABLE OF CONTENTS

LIST OF FIGURES

THIS PAGE INTENTIONALLY LEFT BLANK

LIST OF TABLES

THIS PAGE INTENTIONALLY LEFT BLANK

ACKNOWLEDGMENTS

Life is a never ending challenge. Most of us are living a challenging life and making a better life. When we were born, at first we crawled and later we learned how to walk in spite of falling down. It has been a big challenge for me to study in a different language, abroad, and especially to study physics. Also, it is a great challenge to choose a thesis topic of "Through-the-Wall Imaging using THz". I knew this would not be an easy task, but I chose it and tried to be confident with it. Hence, I have learned lots of things from this.

I would like to thank the Korean government, which gave me a precious opportunity to study at NPS and to live a lovely life with my family. I want to thank my wife who always supported and encouraged me when I was in trouble. Also, I thank my two daughters. They have grown up without any serious health problems, and they have become accustomed to new living conditions and a new school and friends, etc.

I especially want to thank my thesis advisor, Dr. Brett Borden, who gave me essential knowledge and guidance in this research. If not for his help, I could not have written this thesis. Also I want to thank my second reader, Dr. Gamani Karunisiri, who provided valuable insight into the problem. I want to thank LT Jerry Kim whose earlier thesis research provided a starting point for my research.

THIS PAGE INTENTIONALLY LEFT BLANK

I. INTRODUCTION

The amazing ability of terahertz radiation to penetrate through materials allows for the nondestructive, noninvasive inspection of mail and packages in post offices, and luggage at airport security check points [1].

The term terahertz (THz) refers to radiation whose spectrum lies between the infrared and microwave bands with frequencies ranging from 0.1 to 10 THz, where $1\text{THz}=10^{12}\,\text{Hz}$ or, in units of wavelength, $\lambda = 3\,mm$ to $30\,\mu m$. Until recently, this "THz gap" has been almost inaccessible due to the lack of efficient sources and detectors in this region [2]. But recently, sources and detectors for THz frequencies have become available and easier to use. Therefore, many applications of terahertz radiation, such as imaging and communications, are now appearing. Among these applications, a very important application (and the focus of much research) is imaging using THz radiation [3]. The study of this imaging is an interesting and attractive area for researchers.

A. BACKGROUND

Various THz imaging techniques have been developed since Hu and Nuss first demonstrated THz imaging in 1995 [4]. THz imaging applications are the focus of constantly growing interest. Because THz waves can provide great spatial resolution and can penetrate most dielectric materials, such as plastics, paper, and wood, there are many applications of THz imaging. A classical application of THz wave based remote sensing is content inspection of packages and envelopes. Recently, THz imaging has been used for medical and biological applications because it provides high quality images. Another application is real-time nondestructive testing, which includes testing for defects in plastic food and medicine packages. Also, there are a number of security applications for THz imaging: for example, Through-the-Wall Imaging (TWI), luggage inspection, and the detection, from a distance, of weapons or explosives hidden under clothing or briefcases.

B.   MOTIVATION

In the decade between 1996 and 2005, more than a half million servicemen were injured or killed in situations involving barricaded offenders, hostage-taking, and high-risk entry [5]. Through-the-Wall Imaging (TWI) has been studied for saving soldier's and officer's lives. TWI technology can help soldiers to detect enemies hiding in a building, and, for this reason, TWI technology needs to evolve and improve.

The armed forces personnel or police officers who experience operations on urbanized terrain may want equipment that can detect, identify, and localize enemies through a wall, and operate day and night in all weather conditions.

Most imaging systems use bi-static or multi-static transmission, where the transmitter is on one end, and the receiver is on its opposite end. Mono-static systems, on the other hand, use transmitters and receivers that are in the same location. Mono-static imaging systems rely on the back-scattered field. Through-the-wall imaging is more difficult and challenging than any other back scattering method because of the general variability of wall construction. In this thesis, we will concentrate on mono-static imaging techniques.

There are two basic problems in ray-scattering. The first one is the direct scattering problem, which predicts how the rays scatter from a known object. The second is the inverse scattering problem, which attempts to recover the original object from the blurred and corrupted measurements of the scattered field. The inverse scattering problem is one of determining the characteristics of an object from measurement data of radiation or particles scattered from the object. Also, most inverse problems are ill-posed. X-ray, Tomography, and ultra sound imaging are good examples of ill-posed inverse problems.

Let's look at the difference between the direct problem and the inverse problem. The forward problem can be expressed as

$$D = A(f) \qquad\qquad (1.1)$$

in which, we denote the data by $D \in \Box^M$, the object by $f \in \Box^N$ and the operator acting between two spaces containing D and f by A. (N and M denote the dimensions of,

respectively, the object and data spaces and, in general, $N \neq M$.) So the direct problem predicts the data (D) from the object (f). On the other hand, the inverse problem is expressed as

$$f = A^{-1}(D) \tag{1.2}$$

and solves for the object (f) from the data (D). This equation looks easy to solve, but real-world inverse problems are typically much more complicated.

Now let's look at the inverse problem a little bit deeper. If we want to accurately map objects to data, we must also consider the measurement errors. The difference between the actual measurement data (D) and the real data ($\overline{D}$) is denoted by noise $n = \overline{D} - D$, and the scattering problem can be more accurately expressed by

$$\overline{D} = A(f) + n \tag{1.3}$$

The object and data functions are conveniently considered as belonging to Hilbert spaces. In equation (1.3), A is an operator from one Hilbert space to the other. Hilbert space allows simple geometric concepts like projection onto fewer dimensional spaces and loss of information.

Inverse problems are almost always ill-posed problems. J. Hadamard formalized the concept of well-posedness for equations of the form (1.3) [6]. Any equation that does not satisfy all three conditions is called ill-posed, and a method for solving this problem approximately is called a regularization method.

1	Existence	There exists a solution to the problem
2	Uniqueness	There is at most one solution to the problem
3	Stability	The solution depends continuously on the data

Table 1.   Conditions for Well-posed Problems.

C.   PROPERTIES OF TERAHERTZ FREQUENCIES

The term "Terahertz" is applied to broadband pulsed electromagnetic radiation with a spectrum that falls between the infrared and microwave bands ranging from 0.1 to 10 THz [7]. The wavelength in this region ranges from $3\,mm$ to $30\,\mu m$ (as shown in figure 1). These are short wavelengths, and they have high resolution compared to other radio frequencies [2]. There are several distinct advantages of THz waves. The first is that most chemical substances possess characteristic absorption features in the THz range. This property enables us to detect illegal chemicals, even when they are sealed inside a packet or clothing. The second advantage is material transmission properties. Most non-conducting materials such as plastics, paper, wood, and ceramics are totally or partially transparent in the THz range. The third advantage is that the radiation is non-ionizing and has relatively low energies compared to X-rays; therefore, we don't have to be concerned about the safety of THz imaging.

In this thesis, we will use THz pulses for imaging. Figure 2(a) shows examples of THz pulses transmitted through nylon. When a THz pulse interacts with an object, it experiences a delay, an attenuation, and a broadening, as the different component frequencies are phase shifted, absorbed, reflected, and scattered. Figure 2(b) shows the power spectrum that the pulse frequency content is centered around 1THz (note that the higher frequency content is attenuated more than the lower frequencies by nylon).
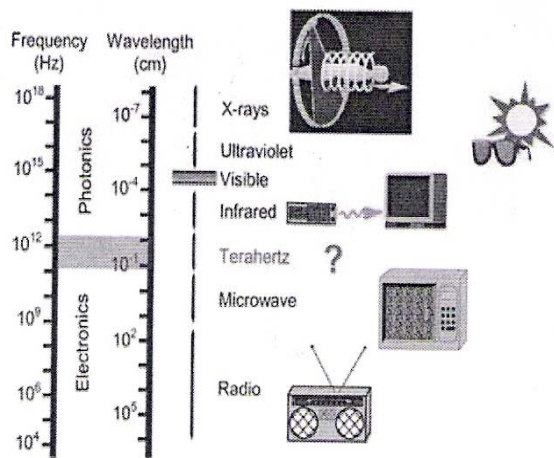
Figure 1.   Electromagnetic spectrum[From 7]

4
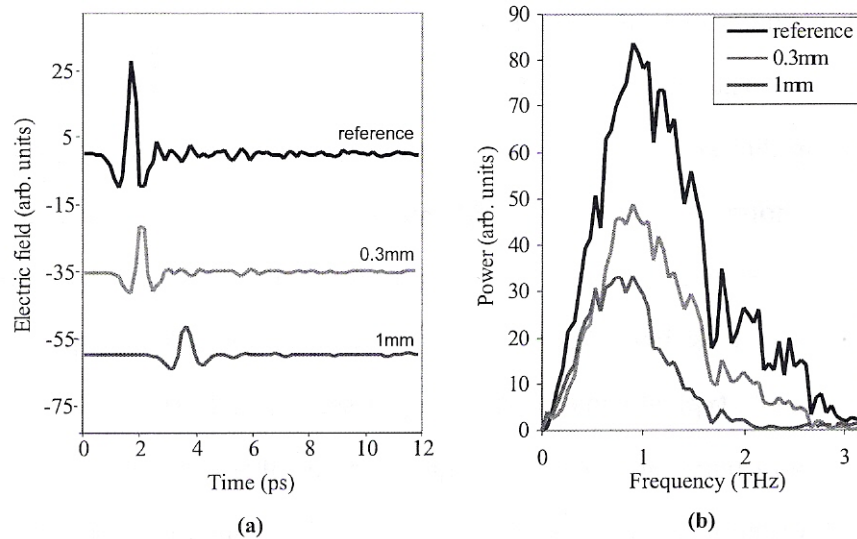
Figure 2.   Examples of terahertz pulses in (a) Time Domain and (b) Magnitude of
Fourier Coefficients [From 4]

For the convenience of modeling, we assume that the wall that we want to see through is a linear, homogeneous, and isotropic dielectric. We know THz frequencies have good penetration for dry materials, but a spectral cut-off above 3 THz will be caused by absorption from water vapor in the THz beam path [8]. So we are not generally interested in frequencies over 3 THz. We also need to consider the object that we want to image. The reflection from the object depends on the object properties. For example, metallic materials reflect perfectly, but skin or water absorbs THz rays, so we can't get significant reflected pulses. Therefore, we should be careful to choose frequencies that balance between the penetration of medium and the reflection of the object.

D.   THESIS ORGANIZATION

This thesis uses Born and Rytov approximations to model measured scattered fields from objects located behind walls.

Chapter II introduces the concept of inverse problems, including ill-posed problems, singular value decomposition, and regularization methods. The Born and Rytov approximations are discussed as well.

Chapter III provides some properties of electromagnetic waves in media and restricts our model system to a real situation. A scalar theory is introduced for use in the succeeding chapters.

Chapter IV develops the transfer function of the media. This chapter describes the mathematical approach and derives Green's functions in different regions.

Chapter V examines reflectives of media and evanescent waves. It also examines materials with reflectivity.

Chapter VI derives a wave equation in the specified medium and the scattered fields by applying the Born and Rytov approximations.

Chapter VII provides algorithms and simulations (with noise) by applying Tikhonov regularization and Truncated Singular Value Decomposition regularization schemes.

Finally, Chapter VIII gives a final summary conclusion, comparing the simulation results and providing suggestions for future work.

II.   THE INVERSE PROBLEM

This chapter will introduce ill-posed problems and regularization solution methods more deeply. Regularization methods are used to mitigate noise effects in the data or the operator. Three widely used regularization techniques are Tikhonov regularization, Truncated Singular Value Decomposition, and regularizing iterative methods. In this thesis, we will use the Tikhonov regularization method and the Truncated SVD method. We will confine ourselves to linear equations with compact operators in Hilbert space and use the Singular Value Decomposition for our reconstruction algorithm design.

A.   REVISIT ILL-POSED PROBLEMS

We want to get images using electromagnetic frequencies. So there is no way to avoid the inverse problem. The very first equation we need is a Lippman-Schwinger equation [9].

$$\psi_{scatt}(x) = \iiint_D G_k(x, x')\rho(x')(\psi_{inc}(x') + \psi_{scatt}(x'))d^3x' \tag{2.1}$$

We denote:

- $G_k(x, x')$ is Green's function which satisfies the wave equation with an impulsive source term

- $\rho(x')$ is a source factor determined by the index of refraction of the scatterer

- $\psi(x)$ is an electric field, $\psi_{inc}(x)$ is the incident field, and $\psi_{scatt}(x)$ is the scattered field

Equation (2.1) is derived from the reduced scalar wave equation

$$\nabla^2\psi(x) + k^2 n^2(x)\psi(x) = 0 \tag{2.2}$$

where $n(x)$ is the index of refraction and k is the wave number.

In this thesis, we ignore multiple scattering. Because we assume multiple scattering terms are very small in comparison to primary scattering, terms we can rewrite equation (2.1) as

$$\psi_{scatt}(x) = \iiint_D G_k(x, x')\rho(x')\psi_{inc}(x')d^3x' \tag{2.3}$$

To get images of objects, we have to estimate $\rho(x)$ (which defines the "image"), but there are some problems. The main problem is that we can never obtain data for all points (x) and at all frequencies (ω). The other problem is that the measurements are always accompanied by noise. If we consider these problems, we can make a more complete measurement model and express equation (2.3) in matrix form. To perform this discritization, we break the integral in equation (2.3) interval $x \in [a\ b]$ into M parts and $x \in [c\ d]$ into N parts. Then the integral equation becomes

$$\int_a^b K(x_i, s)f(s)ds = d(x_i) \quad a \le s \le b, \quad c \le x_1 < x_2 < \cdots < x_N \le d \tag{2.4}$$

where operator K is defined as the kernel which operates on the object $f \in X$ to produce the measurement $d \in Y$. We have simplified equation (2.3) into a one dimensional case and changed notations to better understand this measurement system. Where,

- The measurement at position x_i : $\psi_{scatt}(x_i) \Rightarrow d(x_i)$

- The "kernel" : $G_k(x, x') \Rightarrow K(x_i, s)$

- The "object" function : $\rho(x') \Rightarrow f(s)$

Then we can rewrite equation (2.4) in matrix form (with noise included)as

$$d = Kf + n \tag{2.5}$$

where

8

$$
d = \begin{bmatrix} d(x_1) \\ d(x_2) \\ \vdots \\ d(x_N) \end{bmatrix}, \qquad K = \begin{bmatrix} K(x_1, a+\Delta s) & K(x_1, a+2\Delta s) & \cdots & K(x_1, a+M\Delta s) \\ K(x_2, a+\Delta s) & K(x_2, a+2\Delta s) & \cdots & K(x_2, a+M\Delta s) \\ \vdots & \vdots & \ddots & \vdots \\ K(x_N, a+\Delta s) & K(x_N, a+2\Delta s) & \cdots & K(x_N, a+M\Delta s) \end{bmatrix} \Delta s
$$

$$
f = \begin{bmatrix} f(a+\Delta s) \\ f(a+2\Delta s) \\ \vdots \\ f(a+M\Delta s) \end{bmatrix}, \quad and \quad n = \begin{bmatrix} n(x_1) \\ n(x_2) \\ \vdots \\ n(x_N) \end{bmatrix} \tag{2.6}
$$

and $d \in \mathbb{R}^N$ and $f \in \mathbb{R}^M$ are vectors.

Let's take a close look at the dimension of the measurement space and the object space. The measurement space has dimension N, and the object space has dimension M. This reflects the number N of the discrete measurements and the number N defining the resolution with which f can be estimated. Normally the object dimension M is greater than the measurement of dimension N. Now, equation (2.5) can be used to get f by defining an inverse K^{-1}. However, the noise can alter the measurement space and lead to an unstable estimate of $f = K^{-1}d$. Equation (2.5) is also often an over-determined system, which means there are more equations than unknowns, and we can estimate f by least-squares. Therefore, we have to figure out an over-determined system to get solutions close to the real (discrete) values. We will deal with some methods to get stable solutions in section D.

B. LEAST SQUARES SOLUTION BY SINGULAR VALUE DECOMPOSITION

We consider d to be a vector with components $d_i = d(x_i)$. Normally, the vector of measurements d in equation (2.5) will not lie exactly in the measurement space Y (because of noise). Because $d \in Y$ only if the noise vector $n \in Y$ and $Kf \in Y$. But n is

9
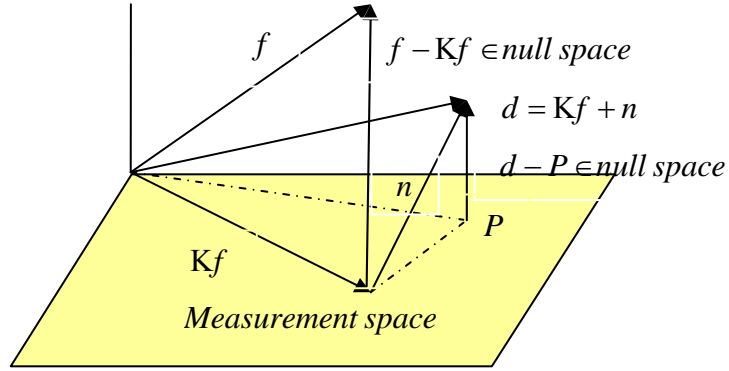
Figure 3.   Hilbert space and measurement space

independent of the operator K, and the object vector f may have components in measurement space or in null space. So a possible "best object" $\tilde{f}$ will minimize the distance $\|d - Kf\|$. We denote the least squares solution to equation as

$$\tilde{f} = \arg\ \min\|d - Kf\| \tag{2.7}$$

From Figure 3 we can get the solution to equation (2.7). The vector Kf lies in measurement space Y. When $K\tilde{f} = P$, Kf gets the closest distance to d. The vector $d - P = d - K\tilde{f}$ is orthogonal to the measurement space Y and all vectors of the form Ky in measurement space Y. Then we can get the normal equations by [10]

$$K^T K \overline{f} = K^T d \tag{2.8}$$

$\overline{f}$ is the least square solution to equation (2.8). Since the matrix $K^T K \in \square^{M \times M}$ is square we can write

$$\overline{f} = (K^T K)^{-1} K^T d \tag{2.9}$$

$\overline{f}$ is exactly what we want. In order to get $\overline{f}$, we have to compute $(K^T K)^{-1} K^T$. But this can be painful to invert with large N and M. So we want to use another method, singular value decomposition, to get $\overline{f}$.

10

We would like to employ simple linear algebra to build matrices of the form $(K^T K)^{-1} K^T$. Consider a matrix A that is square $(M \times M)$ with e_j an eigenvector, λ_j an eigenvalue. We can transform the matrix A in terms of the matrices $e_i e_i^T$, formed from the set of vectors $\{e_i\}$, using the Spectral Theorem which states that A can be written with as

$$A = U \Lambda U^{-1} = U \Lambda U^T = \sum_{i=1}^{M} \lambda_i e_i e_i^T \tag{2.10}$$

where U is the matrix with the eigenvectors of A on its columns and Λ is the matrix with the eigenvalues of A along its diagonal.

We assume $\{e_i\}$ is an orthonomal basis of $\square^M$, and so we can represent an M dimensional vector y in terms of e_i

$$y = \sum_{i=1}^{M} (e_i^T y) e_i = \sum_{i=1}^{M} y_i e_i \tag{2.11}$$

where $y_i = e_i^T y$ is the component of the vector y in the basis. Consequently,

$$x = Ay = \sum_{i=1}^{M} \lambda_i e_i e_i^T y = \sum_{i=1}^{M} \lambda_i y_i e_i = \sum_{i=1}^{M} x_i e_i \tag{2.12}$$

This is representation of $x = Ay$ in terms of the basis $\{e_i\}$.

Let's adjust this result for the matrix $(K^T K)^{-1} K^T$. Suppose $\{e_j\}$ are the eigenvectors of $K^T K$. Then

$$(K^T K)^{-1} = (U \Lambda U^{-1})^{-1} = U \Lambda^{-1} U^T \tag{2.13}$$

Multiply by K^T on the right of both sides

$$(K^T K)^{-1} K^T = U \Lambda^{-1} U^T K^T = U \Lambda^{-1} (KU)^T$$

$$= U \Lambda^{-1} \left(\begin{bmatrix} \vdots & \vdots & & \vdots \\ Ke_1 & Ke_2 & \cdots & Ke_m \\ \vdots & \vdots & & \vdots \end{bmatrix} \right)^T$$

$$= U \underbrace{\begin{bmatrix} \sigma_1/\lambda_1 & 0 & \cdots & 0 \\ 0 & \sigma_2/\lambda_2 & \cdots & 0 \\ \vdots & \vdots & \ddots & \vdots \\ 0 & 0 & \cdots & \sigma_M/\lambda_M \end{bmatrix}}_{D} \underbrace{\begin{bmatrix} \cdots & \hat{e}_1^T & \cdots \\ \cdots & \hat{e}_2^T & \cdots \\ \vdots & \vdots & \vdots \\ \cdots & \hat{e}_M^T & \cdots \end{bmatrix}}_{V^T} \qquad (2.14)$$

$$= UDV^T$$

We define $\sigma_i \equiv \|Ke_i\|$ and $\sigma_i \equiv \hat{e}_1 = \begin{cases} \sigma_i^{-1} Ke_i & if\ \sigma_i \neq 0 \\ 0 & if\ \sigma_i = 0 \end{cases}$

Now multiply both sides of equation (2.9) by K so that

$$K\overline{f} = K(K^T K)^{-1} K^T d = P \qquad (2.15)$$

P is the projection of the measurement vector onto measurement space. Therefore, $K(K^T K)^{-1} K^T$ is a projection matrix mapping d to its components in measurement space. We will use this projection matrix to get more accurate data using regularization techniques in the following section.

C.   TRUNCATED SINGULAR VALUE DECOMPOSITION

To obtain a better estimate of the least square solution, the truncated singular value decomposition solution is often used. This method truncates the SVD representation to reduce the effect of noise contamination. Just select one small threshold value $\mathcal{K}$ and compare this with singular values λ_i. If $\mathcal{K} > \lambda_i$, then we replace the $1/\sqrt{\lambda_i}$ in D by 0. In this thesis, using the plot of singular values, we will find the critical point where the singular values change steeply and will truncate at that point [11] (see Figure 21).

D.   REGULARIZATION METHODS

Since our model is linear and ill-posed, the inverse image is under-determined, and we will get small singular values of K. The problem is that K depends on our model of the measurement process and is not completely known. So we get singular values with a slight imprecision. Now we introduce regularization methods to overcome the problems associated with the small singular values that lead to reconstruction instability. Regularization is important for solving inverse problems, because the output of least squares is affected by data and rounding errors. Therefore we would like to introduce regularization methods to reduce these errors. But there is a trade-off between the regularized output and the original sets of data. If the regularization is too crude, the regularized solution does not fit the given data, and the residual error $\|r\| = \|d - \mathrm{K}f\|$ is unnecessarily large. If the regularization is too small, the fit will be good, but data noise effects will be larger.

There are also some regularization methods that employ operator or data correction [12].

1.   Regularization by Operator Correction

Let's model the problem by mapping A as

$$Ax = d, \quad x \in X, \quad d \in Y \tag{2.16}$$

The equation (2.16) is said to be an ill-posed problem, if it does not meet one of the conditions in table I. If we want to transform an ill-posed problem into a well-posed problem by approximation of the equation, then we have to choose a mapping method.

The regularization of equation (2.16) consists of a substitution of the operator A by $\tilde{A}$. Let $\tilde{A} \cdot X \to Y$ be an operator such that

$$\tilde{A}x = d \tag{2.17}$$

This is the idea behind the well known Tikhonov regularization.

2.   Regularization by Data Correction

Let $K \cdot Y \rightarrow A$ be a continuous operator such that

then

$$Ax = Kd, \quad x \in X, \quad d \in Y \qquad (2.18)$$

is well-posed and called as regularization by data correction.

3.   Regularization by Data and Operator Correction

The last method of regularizations is a combination of both previous methods. Let $\tilde{A} \cdot X \rightarrow Y$ be an operator and $K \cdot Y \rightarrow Y$ a continuous mapping such that

$$\tilde{A}x = Kd, \quad x \in X, \quad d \in Y \qquad (2.19)$$

Tikhonov regularization is also a well known method of this kind of regularization.

E.   L-CURVE METHOD

Since the quality of the regularized solution is controlled by the regularization parameter for example, the threshold parameter $\mathcal{K}$ used in truncated SVD regularization [13], we have to choose the optimal parameter to get a "best" image. There are various methods for the selection of regularization parameters, including the Discrepancy Principle, Generalized Cross Validation, and L-curve. The L-curve method applies a log-log plot of the regularized solution against the squared norm of the regularized residual for a range of values of regularization parameters [13] and selects the corner as the point of maximum curvature in the L-curve plot (see Figure 4).

There are two main approaches used in the L-curve method. The first approach considers both the residual norm and the solution norm. The second approach considers the value of the maximum curvature. Like other methods, the L-curve method has its merits and limitations. The merits of L-curve are that it's robust and can treat perturbation caused by correlation noise. On the other hand, the L-curve method is

limited, because it is not convergent [14], i.e., since singular values are getting close to 0 but not exactly 0 as increasing index of singular values, we can't get the value which satisfies the norm is 0.
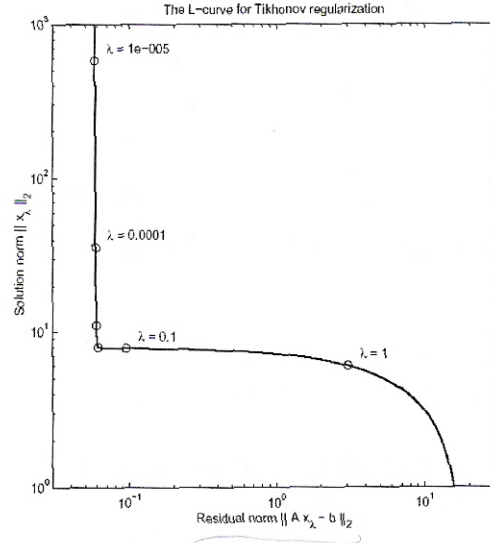
Figure 4.   L-curve for Tikhonov Regularization [From 14]

F.   APPROXIMATIONS TO THE WAVE EQUATION

In the case of electromagnetic scattering problems, we need to approximate the unknown internal field by a known distribution in order to linearize the problem. The Born and Rytov approximations are widely used to simplify electromagnetic scattering problems. In this thesis we will derive reconstruction formulas under the Rytov approximation and compare with the Born approximation.

1.   Born Approximation

The first Born approximation was introduced by Max Born in 1925, in order to solve problems concerning the scattering of atomic particles [7]. The Born approximation is obtained by expressing the total wave field as the sum of incident field plus scattered field:

$$\psi(r) = \psi_i(r) + \psi_s(r) \tag{2.20}$$

15

This approximation assumes that scattered fields inside scatterers are negligible compared to the background and the normal fields. The first-order Born approximation is good only if the scattered field is much smaller than the incident field.

2.   Rytov Approximation

The Rytov approximation was discovered in 1937 by Rytov, who was analyzing the diffraction of light by sound waves. This approximation was later applied by Obukhov to describe the propagation of electromagnetic waves in random media [15]. The Rytov approximation is based on expressing the total field as a complex phase, which is the sum of incident phases plus scattered phases:

$$\psi(r) = e^{\phi(r)} = e^{\phi_i(r)+\phi_s(r)} \tag{2.21}$$

The condition for the applicability of this approximation is that the phase of the scattered field varies slowly, relative to one wavelength. So the size of target is less critical in the Rytov approximation.

III.   ELECTROMAGNETIC WAVES IN MEDIA

It is difficult to explain electric fields and magnetic fields, which are cross-coupled, without the Maxwell's equations. Maxwell's equations were established by James Clerk Maxwell by 1864 and experimentally verified by Heinrich Hertz in 1888 [16]. Since then these equations have been applied in a variety of areas such as optics, microwaves, antennas, radar, and communications. In this chapter we will investigate Maxwell's equations in media and derive the associated wave equations.

A.   MAXWELL'S EQUATIONS

Maxwell's equations are comprised of Gauss' law for the electric field, the observation that there are no magnetic monopoles, Ampere's law, including the displacement current $\dfrac{\partial D}{\partial t}$, and Faraday's law of induction in differential form. They can be written as

$$
\begin{aligned}
\nabla \cdot D &= \rho \\
\nabla \cdot B &= 0 \\
\nabla \times E &= -\frac{\partial B}{\partial t} \\
\nabla \times H &= J + \frac{\partial D}{\partial t}
\end{aligned}
\tag{3.1}
$$

where D and B are the electric and magnetic flux intensities, and E and H are the electric and magnetic field intensities, J is electric current density, and ρ is volume charge density. In reality, there are two more things we have to consider for Maxwell's equations. These are P, and M, called induced polarization and magnetization respectively. The associated constitutive relations are expressed as

$$
D = \varepsilon_0 E + P
\tag{3.2}
$$

$$
B = \mu_0 (H + M)
\tag{3.3}
$$

17

Using equations (3.2) and (3.3), we can rewrite Maxwell's equations in terms of E and B.

$$\nabla \cdot E = \frac{1}{e_0}(\rho - \nabla \cdot P)$$
$$\nabla \cdot B = 0$$
$$\nabla \times E = -\frac{\partial B}{\partial t} \qquad (3.4)$$
$$\nabla \times B = \mu_0 e_0 \frac{\partial E}{\partial t} + \mu_0 \left[J + \frac{\partial P}{\partial t} + \nabla \times M \right]$$

where μ_0 and e_0 are the permeability and permittivity in free space, respectively. The speed of light (c) and characteristic impedance (η_0) of a vacuum are expressed using μ_0 and e_0 as

$$c = \frac{1}{\sqrt{\mu_0 e_0}}, \qquad \eta_0 = \sqrt{\frac{\mu_0}{e_0}} \qquad (3.5)$$

1.   Simplified Model

Electromagnetic fields behave differently in the presence of media. For Through the Wall Imaging using electromagnetic waves, we will confine our attention to materials obeying a linear model. Materials used for constructing walls include wood, concrete, and iron-beams. These materials typically have anisotropic permittivity. Anisotropic is an inherent property of the atomic and molecular structure of the dielectric [17]. So in anisotropic materials, permittivity depends on its direction and the linear constitutive relation can be written in matrix form as

$$\begin{bmatrix} D_x \\ D_y \\ D_z \end{bmatrix} = \begin{bmatrix} e_{xx} & e_{xy} & e_{xz} \\ e_{yx} & e_{yy} & e_{yz} \\ e_{zx} & e_{zy} & e_{zz} \end{bmatrix} \begin{bmatrix} E_x \\ E_y \\ E_z \end{bmatrix} \qquad (3.6)$$

In general, the field vector E is no longer parallel to D. But we can simplify our model by using the principal axis system: We consider homogeneous and linear materials so that the permittivity is independent of position. Then the permittivity tensor can be expressed with six elements as

18

$$tensor(\mathbf{e}) = \begin{bmatrix} \mathbf{e}_{xx} & \mathbf{e}_{xy} & \mathbf{e}_{xz} \\ \mathbf{e}_{xy} & \mathbf{e}_{yy} & \mathbf{e}_{yz} \\ \mathbf{e}_{xz} & \mathbf{e}_{yz} & \mathbf{e}_{zz} \end{bmatrix} \tag{3.7}$$

Since this matrix is symmetric, its eigenvectors are orthogonal. If we choose a coordinate system which is aligned to these eigenvectors, we can rewrite the permittivity tensor as a diagonal tensor determined by its eigenvalues. Then equation (3.7) becomes

$$tensor(\mathbf{e}) = \begin{bmatrix} \mathbf{e}_{xx} & 0 & 0 \\ 0 & \mathbf{e}_{yy} & 0 \\ 0 & 0 & \mathbf{e}_{zz} \end{bmatrix} \tag{3.8}$$

Let's investigate solutions to the Maxwell's equations for source free homogeneous isotropic media. Here, $J = \rho = 0$ and Maxwell's equations (3.4) become

$$\nabla \cdot E = 0, \quad \nabla \times E + \frac{\partial B}{\partial t} = 0,$$
$$\nabla \cdot B = 0, \quad \nabla \times B - \mu \mathbf{e} \frac{\partial E}{\partial t} = 0 \tag{3.9}$$

To derive the wave equation we first take the curl of the second of equation (3.9)

$$\nabla \times (\nabla \times E) + \nabla \times \frac{\partial B}{\partial t} = 0 \tag{3.10}$$

$$\nabla \times (\nabla \times E) + \frac{\partial}{\partial t}(\nabla \times B) = 0 \tag{3.11}$$

and use the identity of $\nabla \times (\nabla \times E) = \nabla(\nabla \cdot E) - \nabla^2 E = -\nabla^2 E$, since we assume a charge free and homogeneous region that means $\nabla \cdot E = 0$, and we obtain

$$-\nabla^2 E + \frac{\partial}{\partial t}(\nabla \times B) = 0 \tag{3.12}$$

Now take the partial derivative with respect to t of the forth of equation (3.9)

$$\nabla \times \frac{\partial B}{\partial t} - \mu \mathbf{e} \frac{\partial^2 E}{\partial t^2} = 0 \quad \Rightarrow \quad \frac{\partial}{\partial t}(\nabla \times B) = \mu \mathbf{e} \frac{\partial^2 E}{\partial t^2} \tag{3.13}$$

and substitute this into equation (3.12) to obtain

19

$$\nabla^2 E - \mu e \frac{\partial^2 E}{\partial t^2} = 0 \tag{3.14}$$

The plane wave solutions to equation (3.14) can be written as

$$\vec{E}(r,t) = \vec{E}_0 e^{i(\vec{k}\cdot\vec{r}-\omega t)} \tag{3.15}$$

Substituting equation (3.15) into equation (3.14) we find the following equation

$$k^2 = \omega^2 \mu e \tag{3.16}$$

This is called as the dispersion relation. We can easily find the phase velocity as

$$\omega/k = 1/\sqrt{\mu e} \tag{3.17}$$

For conductive materials with permittivity $e + i\sigma/\omega$, the wave number is complex and written as [16]

$$k = k_R + ik_I$$
$$\simeq \omega\sqrt{\mu e}\left[i\frac{\sigma}{\omega e}\right]^{1/2} = (1+i)\sqrt{\frac{\omega\mu\sigma}{2}} \tag{3.18}$$

Then the penetration depth is

$$d_p = \frac{1}{k_I} = \sqrt{\frac{2}{\omega\mu\sigma}} \tag{3.19}$$

For a wave propagating in the $+\hat{z}$ direction, we have z dependence given by

$$e^{-ikz} = e^{-ik_R z - ik_I z} \tag{3.20}$$

This wave attenuates exponentially in the same direction that it propagates. Figure 5 shows a wave propagating in a lossy medium.

For a highly conducting medium with $1 \ll \dfrac{\sigma}{\omega e}$, the penetration depth is a very small. So the waves will not be able to penetrate conductive materials. Therefore we ignore highly conductive materials in this thesis.
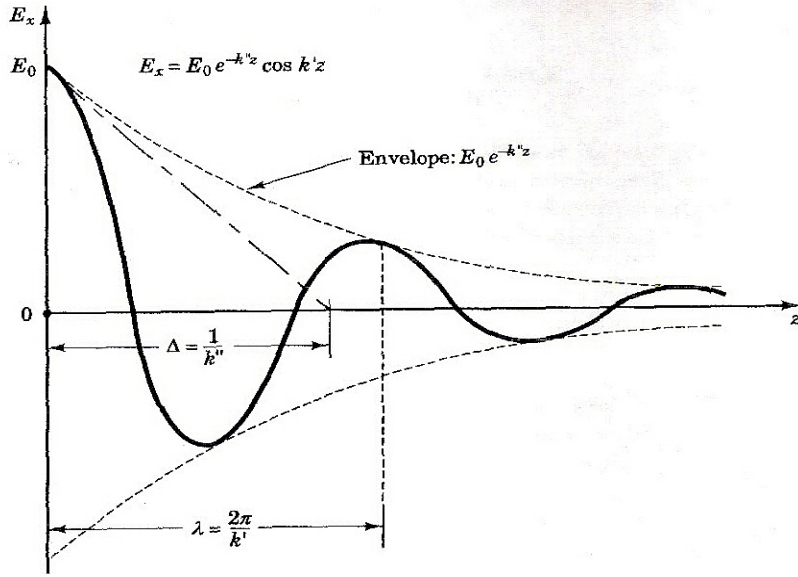
Figure 5.   Wave propagating in a lossy medium[From 18]

2.   Properties of Frequency and Dispersion

When the electric field is applied to a dielectric, the electric field tends to separate the electron from the positively charged nucleus, and this creates an electric dipole moment. Moreover, the dipole moment contributes to the electric flux density so that

$$D = \varepsilon_0 E + P = \varepsilon_0 (1 + \chi(\omega)) E = \varepsilon(\omega) E \tag{3.21}$$

where $\chi(\omega)$ is susceptibility. From equation (3.21) we can see the permittivity is changed because of the dipole moment. The polarization of a medium with refractive index n is

$$\vec{P} = \chi \varepsilon_0 \vec{E} \tag{3.22}$$

and the susceptibility is expressed as [16]

$$\chi = \frac{nq^2}{m\varepsilon_0 (\omega_0^2 - \omega^2 - i\gamma)} \tag{3.23}$$

21

where $\gamma = \frac{1}{\tau}$, which is a measure of the rate of collisions per unit time. Rationalizing Equation (3.23) as

$$\chi = \frac{nq^2 \left[\left(\omega_0^2 - \omega^2 \right) + i\omega\gamma \right]}{m\mathrm{e}_0 \left[\left(\omega_0^2 - \omega^2 \right)^2 + \omega^2\gamma^2 \right]}$$ (3.24)

and substituting equation (3.24) into equation (3.21), we get the permittivity as

$$\mathrm{e} = \mathrm{e}_0 + \frac{nq^2 \left(\omega_0^2 - \omega^2 \right)}{m \left[\left(\omega_0^2 - \omega^2 \right)^2 + \omega^2\gamma^2 \right]} + \frac{inq^2\omega\gamma}{m \left[\left(\omega_0^2 - \omega^2 \right)^2 + \omega^2\gamma^2 \right]}$$ (3.25)

When ω is not close to ω_0, the imaginary term will be much smaller than the real term. This means e is approximately real valued when ω is not very near resonance. When not close to a resonance, the deviation of the refractive index from unity is

$$n - 1 \simeq \frac{nq^2}{2m\mathrm{e}_0 \left(\omega_0^2 - \omega^2 \right)} \left(1 + \frac{i\omega\gamma}{\omega_0^2 - \omega^2} \right)$$ (3.26)

From equation (3.26) the real part of n represents dispersion and the imaginary part represents absorption. Figure 6 shows us that around the resonant frequency ω_0, the real part of n behaves in a strange manner and drops rapidly with frequency, and the material absorption occurs quite high. So we have to avoid choosing a radiation frequency that is in resonance with the dielectric.

To make our model system more numerically tractable, we need more assumptions. Dispersive media have values of μ, e and σ that depend on frequency. As a result, the wave velocity is generally frequency-dependent [18]. So, dispersive media have frequency-dependent constitutive laws; this means waves of different frequencies propagate with different velocities. For dispersive media, we need lots of information about different materials. The analysis is complex and unnecessary. So we will not consider highly dispersive media in this thesis.

22
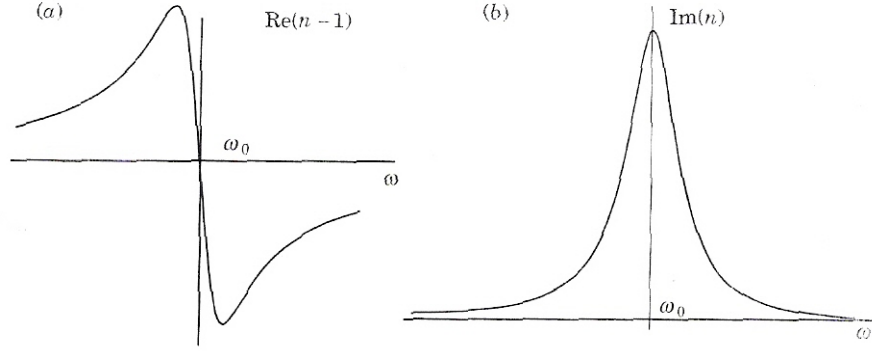
Figure 6.   Real and imaginary parts of the refractive index [From 19]

In general, the velocity of the envelope of any modulated sinusoid is the group velocity v_g which is the speed at which energy and information travel [18].

$$v_g = \left(\frac{\partial k}{\partial \omega} \right)^{-1} \tag{3.27}$$

For these reasons, our model assumes that the media have low conductivity and are non-dispersive.

B.   THE SCALAR THEORY

In the previous section, we derived the vector wave equation (3.14). Also, we restricted our model to a dielectric medium that is linear, homogeneous, isotropic, and non-dispersive. If the medium is just like that, we can rewrite the wave equation for the electric field as

$$\nabla^2 \mathbf{E} - \frac{n^2}{c^2} \frac{\partial^2 \mathbf{E}}{\partial t^2} = 0 \tag{3.28}$$

Identically, we get the same equation for the magnetic field as

$$\nabla^2 \mathbf{H} - \frac{n^2}{c^2} \frac{\partial^2 \mathbf{H}}{\partial t^2} = 0 \tag{3.29}$$

Since these are vector equations, we will get 6 equations with 6 components: E_x, E_y, E_z and H_x, H_y, H_z. But fortunately, we can make these equations into a single scalar wave

23

equation because under our model restriction, all vector components of $\mathbf{E}$ and $\mathbf{H}$ are identical. A single wave equation becomes

$$\nabla^2 \psi(x,t) + \frac{n^2}{c^2}\frac{\partial^2 \psi(x,t)}{\partial t^2} = 0 \tag{3.30}$$

where $\psi(x,t)$ represents any of the vector field components and ψ is dependent on position x and time t. However, when the medium is inhomogeneous with a permittivity $e(x)$ that depends on position x, then the wave equation is not the same as before. The wave equation is derived by the following procedures. First we consider the first line of equation (3.1) and equation (3.21). Combining these equations yields

$$e\nabla \cdot \mathbf{E} + (\nabla e) \cdot \mathbf{E} = \rho \tag{3.31}$$

Divide by e on both sides

$$\nabla \cdot \mathbf{E} = \frac{\rho}{e} - \frac{(\nabla e) \cdot \mathbf{E}}{e} = \frac{\rho}{e} - (\nabla \ln e) \cdot \mathbf{E} \tag{3.32}$$

Now take curl of the third of equation (3.1)

$$\nabla \times (\nabla \times \mathbf{E}) = -\nabla \times \frac{\partial \mathbf{B}}{\partial t} \tag{3.33}$$

$$\nabla(\nabla \cdot \mathbf{E}) - \nabla^2\mathbf{E} = -\frac{\partial}{\partial t}\left(\nabla \times (\mu\mathbf{H})\right) \tag{3.34}$$

And substitute equation (3.32) into equation (3.34)

$$\nabla\left[\frac{\rho}{e} - (\nabla \ln e) \cdot \mathbf{E}\right] - \nabla^2\mathbf{E} = -\frac{\partial}{\partial t}\left(\nabla \times (\mu\mathbf{H})\right) \tag{3.35}$$

One of the laws for operations with the div-and-curl operator is

$$\nabla \times (\phi F) = \phi\nabla \times F + (\nabla \phi) \times F \tag{3.36}$$

and so equation (3.35) becomes

$$\nabla^2\mathbf{E} - \nabla\frac{\rho}{e} + \nabla\left[(\nabla \ln e) \cdot \mathbf{E}\right] = \left[\mu\frac{\partial}{\partial t}\left(\nabla \times \mathbf{H}\right)\right] + \frac{\partial}{\partial t}\left[(\nabla \mu) \times \mathbf{H}\right] \tag{3.37}$$

24

Using the fourth line in equation (3.1), equation (3.37) becomes

$$\nabla^2 \mathbf{E} - \epsilon\mu \frac{\partial^2 \mathbf{E}}{\partial t^2} + \left[\nabla(\nabla \ln \epsilon)\cdot\mathbf{E}\right] = \nabla\frac{\rho}{\epsilon} + \frac{\partial}{\partial t}\left[(\nabla\mu)\times\mathbf{H}\right] \tag{3.38}$$

For nonmagnetic material, $\mu = \mu_0$. When $\rho = 0$, equation (3.38) can be simplified to

$$\nabla^2 \mathbf{E} + \nabla\left[(\nabla \ln \epsilon)\cdot\mathbf{E}\right] - \epsilon\mu \frac{\partial^2 \mathbf{E}}{\partial t^2} = 0 \tag{3.39}$$

Finally, with the help of the refractive index, $n^2 = \epsilon/\epsilon_0$, and the speed of light in vacuum, $c^2 = 1/\epsilon_0\mu_0$, equation (3.39) becomes

$$\nabla^2 \mathbf{E} + 2\nabla\left[\nabla(\ln n)\cdot\mathbf{E}\right] - \frac{n^2}{c^2}\frac{\partial^2 \mathbf{E}}{\partial t^2} = 0 \tag{3.40}$$

The extra term in equation (3.40), $2\nabla\left[\nabla(\ln n)\cdot\mathbf{E}\right]$, will not be zero when n varies with position. So electric fields E_x, E_y and E_z may not satisfy the same wave equation. Consequently, we can't make these vector waves into a single scalar wave. Also, we will get some error by using scalar theory, even in the homogeneous medium when the boundary conditions are imposed on a wave [20].

We will consider scalar components and the corresponding scalar wave equation instead of the full vector theory in the thesis.

THIS PAGE INTENTIONALLY LEFT BLANK

IV. THE TRANSFER FUNCTION

For the purpose of our model, we have to develop the transfer function of a wall-like medium. We assume that the wave propagates into the medium with an index of refraction (n_m). The source is located at $r_0 = -z_0 \hat{z}$, and coordinates are as shown in Figure 7.

The scalar wave equation with source $s(r,t)$ in the time domain becomes

$$\nabla^2 E - \frac{n^2}{c^2}\frac{\partial^2 E}{\partial t^2} = s(r,t) \tag{4.1}$$

Using the Inverse Fourier Transform, we can express the source term in terms of angular frequency (ω) and oscillation frequency (ν) as

$$s(r,t) = \frac{1}{2\pi}\int_{-\infty}^{\infty} S(r,\omega)e^{i\omega t}d\omega \tag{4.2}$$

where $S(r,\omega)$ is the source term in the angular frequency domain.

Using the identity $\omega = 2\pi\nu$ and $d\omega = 2\pi d\nu$, equation (4.2) becomes

$$s(r,t) = \int_{-\infty}^{\infty} S(r,\nu)e^{i2\pi\nu t}d\nu \tag{4.3}$$

where $S(r,\nu)$ is the source term in the oscillation frequency domain.

In the previous chapter, we showed that a plane wave solution is in the form of equation (3.15). This will satisfy equation (4.1), and we can obtain the following relationship.

$$\partial E^2 \Big/ \partial t^2 = -\omega^2 E \tag{4.4}$$

Then we can make equation (4.1) into a time independent wave equation as

$$\nabla^2 E + n^2 k^2 E = S(r,\nu) \tag{4.5}$$

To get the solution of equation (4.5), we put the source at the point $r_0 = -z_0\hat{z}$ and use the Green's function which satisfies the following equation

27
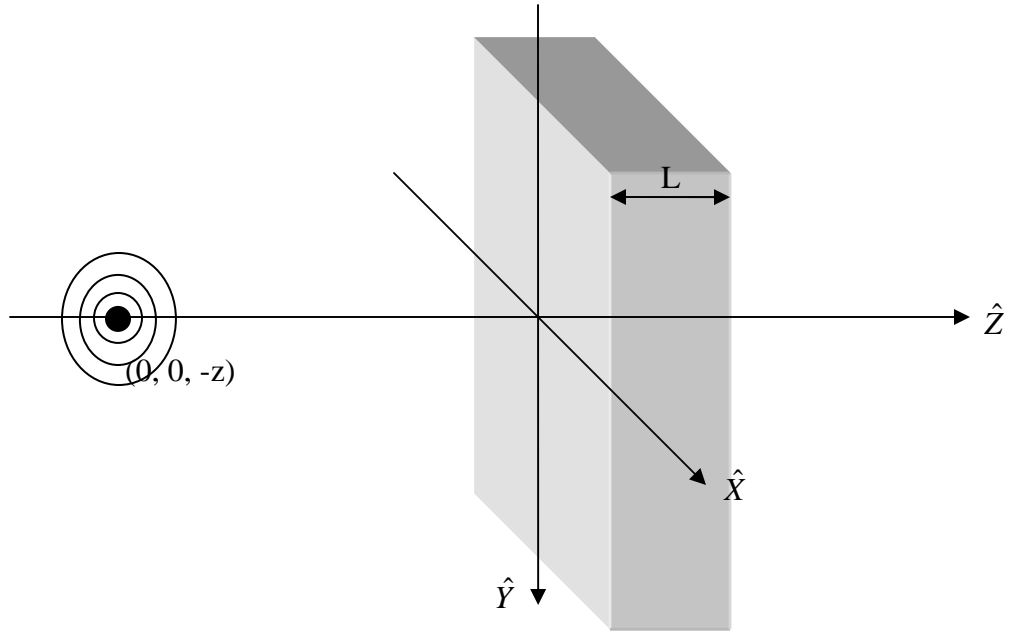
Figure 7.   Point source emanating waves through a medium

$$(\nabla^2 + k^2 n^2(z))g(r,r_0) = \delta(r+r_0) = \delta(x)\delta(y)\delta(z+z_0) \qquad (4.6)$$

where $k = \dfrac{2\pi}{\lambda}$ and λ is the wavelength in free-space.

The refractive index of our system is

$$n(z) = \begin{cases} 1 & for \quad z < 0 \\ n & for\ 0 \le z \le L \\ 1 & for \quad L < z \end{cases} \qquad (4.7)$$

Then we can get the solution for E in the frequency domain as

$$E(r,v) = \int g(r,r_0)S(r,v)d^3r_0 \qquad (4.8)$$

Where $g(r,r_0)$ is the Green's function in the spatial domain, and the solution for E in the time domain (using the Inverse Fourier Transform) as

$$E(r,t) = \int_{-\infty}^{\infty} E(r,v)e^{i2\pi vt}dv \qquad (4.9)$$

In our model, we assume that the medium is essentially non-conductive, so the electromagnetic wave can propagate the medium with little damping. Since we put the source at $r_0 = -z_0 \hat{z}$ along the $\hat{z}$ direction we can convert the equation (4.6) into the Fourier domain.

$$G(v_x, v_y, z, r_0) \equiv \int_{-\infty}^{\infty} \int_{-\infty}^{\infty} g(x, y, z, r_0) e^{-i(2\pi v_x x + 2\pi v_y y)} dx dy \qquad (4.10)$$

$$g(x, y, z, r_0) \equiv \int_{-\infty}^{\infty} G(v_x, v_y, z, r_0) e^{i(2\pi v_x x + 2\pi v_y y)} dv_x dv_y \qquad (4.11)$$

These expressions are correct in our model, because the medium remains constant in the x and y direction. Therefore, there is no changing of the medium in these directions.

Now substituting equation (4.11) into equation (4.6) and using the identity in equation (4.10), we obtain

$$\left[-(2\pi v_x)^2 - (2\pi v_y)^2 + \frac{\partial^2}{\partial z^2} \right] G(v_x, v_y, z, r_0) + k^2 n^2(z) G(v_x, v_y, z, r_0) = \delta(z + z_0) \quad (4.12)$$

If we define

$$F \equiv 2\pi v_x \hat{x} + 2\pi v_y \hat{y} \qquad (4.13)$$

we get

$$|F|^2 = (2\pi v_x)^2 + (2\pi v_y)^2 \qquad (4.14)$$

Using the wave number definition, we can rewrite

$$k^2 = k_x^2 + k_y^2 + k_z^2 = \left(\frac{2\pi}{\lambda_x}\right)^2 + \left(\frac{2\pi}{\lambda_y}\right)^2 + \left(\frac{2\pi}{\lambda_z}\right)^2 \qquad (4.15)$$
$$= (2\pi v_x)^2 + (2\pi v_y)^2 + (2\pi v_z)^2$$

$$v_x = \frac{1}{\lambda_x}, \quad v_y = \frac{1}{\lambda_y}, \quad v_z = \frac{1}{\lambda_z}$$

If $z \neq -z_0$, the equation (4.12) becomes the homogeneous wave equation as
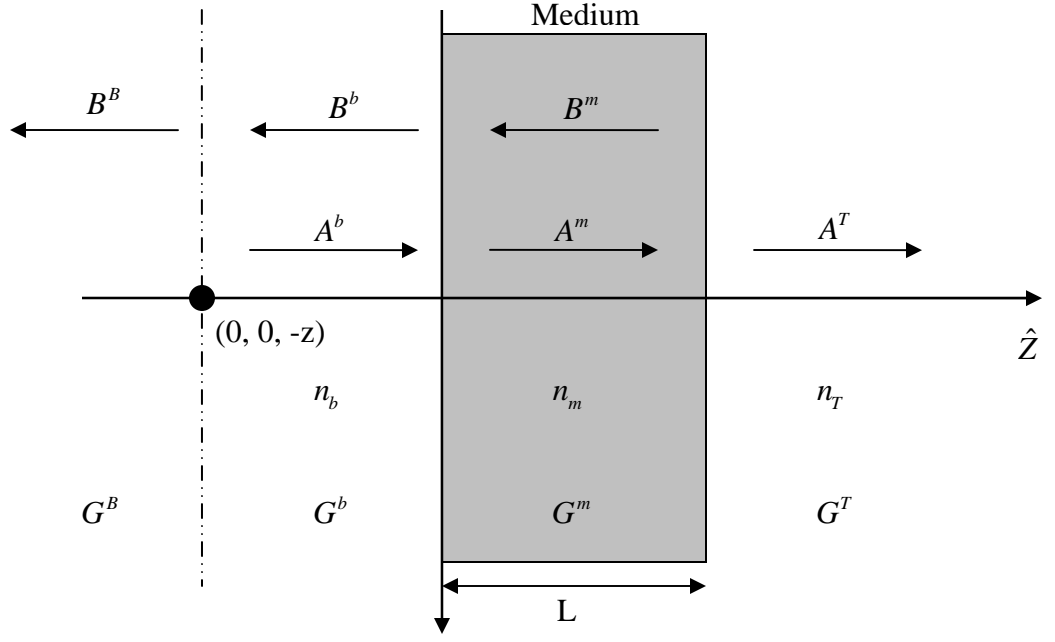
Figure 8.   Cross sectional view of the wave front

$$\frac{\partial^2}{\partial z^2} G(v_x, v_y, z, r_0) + \left[k^2 n^2(z) - |F|^2 \right] G(v_x, v_y, z, r_0) = 0 \qquad (4.16)$$

So this solution becomes

$$G(v_x, v_y, z, r_0) = \underbrace{A e^{iz\sqrt{k^2 n^2(z) - |F|^2}}}_{right\ going\ wave} + \underbrace{B e^{-iz\sqrt{k^2 n^2(z) - |F|^2}}}_{left\ going\ wave} \qquad (4.17)$$

The solutions of the wave equations in each region must satisfy the boundary conditions, which state that the wave and its derivatives must be continuous at all boundaries. Then we can find the coefficients of each component wave as they propagate through the medium (Figure 8).

The boundary conditions are

$$G^B \Big|_{z=-z_0} = G^b \Big|_{z=-z_0} \quad , \quad \frac{\partial G^b}{\partial z} \Big|_{z=-z_0} - \frac{\partial G^B}{\partial z} \Big|_{z=-z_0} = 1 \qquad (4.18)$$

$$G^b \Big|_{z=0} = G^m \Big|_{z=0} \quad , \quad \frac{\partial G^b}{\partial z} \Big|_{z=0} = \frac{\partial G^m}{\partial z} \Big|_{z=0} \qquad (4.19)$$

$$G^m\big|_{z=L} = G^T\big|_{z=L} \quad, \quad \frac{\partial G^m}{\partial z}\bigg|_{z=L} = \frac{\partial G^T}{\partial z}\bigg|_{z=L} \tag{4.20}$$

We can ignore the coefficient A^B of the left going component at $z < -z_0$ and B^T of the right going component at $z > L$, because the wave is outgoing from the source. In addition, by imposing the Sommerfeld radiation condition, the surface integral at infinity vanishes [16]. Since the waves are continuous, the Green's functions and its derivatives also have to be continuous, except at the source. Let's find the derivative of the Green's function. We use equation (4.12) and integrate it on both sides.

$$\int \frac{\partial^2}{\partial z^2} G(v_x, v_y, z, r_0)dz + \int (k^2 n^2(z)) - (2\pi v_x)^2 - (2\pi v_y)^2 G(v_x, v_y, z, r_0)dz = \int \delta(z + z_0)dz \tag{4.21}$$

The left hand side becomes the first derivative of the Green's function and an integral of the Green's function. The right hand side is the same as the Heaviside Step Function, which is a discontinuous function whose value is zero for negative argument and one for positive argument. Then the equation becomes

$$\frac{\partial}{\partial z} G(v_x, v_y, z, r_0) + \int (k^2 n^2(z) - (2\pi v_x)^2 - (2\pi v_y)^2)G(v_x, v_y, z, r_0)dz = H(z + z_0) \tag{4.22}$$

The second term in equation (4.22) will vanish, because the Green's function is continuous at any given boundary. But the first term will be continuous as long as the boundaries are $z < -z_0$ or $z > -z_0$. As the first derivative crosses the source where the Heaviside Step Function goes from 0 to 1, the difference across will jump to 1. Using the same boundaries as the above, we get the following:

If we let the refractive index obey

$$n_b \quad (z < 0)$$
$$n_m \quad (0 \le z \le L)$$
$$n_T \quad (L < z)$$

then, we can derive the following equations:

At $z = 0$

$$A^b + B^b = A^m + B^m \tag{4.23}$$

$$A^b \sqrt{k^2 n_b^2 - |F|^2} - B^b \sqrt{k^2 n_b^2 - |F|^2} = A^m \sqrt{k^2 n_m^2 - |F|^2} - B^m \sqrt{k^2 n_m^2 - |F|^2} \tag{4.24}$$

$$\underbrace{\begin{bmatrix} 1 & 1 \\ \sqrt{N_b} & -\sqrt{N_b} \end{bmatrix}}_{M_1} \begin{bmatrix} A^b \\ B^b \end{bmatrix} = \underbrace{\begin{bmatrix} 1 & 1 \\ \sqrt{N_m} & -\sqrt{N_m} \end{bmatrix}}_{M_2} \begin{bmatrix} A^m \\ B^m \end{bmatrix} \tag{4.25}$$

where $N_b = k^2 n_b^2 - |F|^2$ and $N_m = k^2 n_m^2 - |F|^2$

At $z = L$

$$A^m e^{iL\sqrt{k^2 n_m^2 - |F|^2}} + B^m e^{-iL\sqrt{k^2 n_m^2 - |F|^2}} = A^T e^{iL\sqrt{k^2 n_T^2 - |F|^2}} \tag{4.26}$$

$$A^m \sqrt{k^2 n_m^2 - |F|^2}\, e^{iL\sqrt{k^2 n_m^2 - |F|^2}} - B^m \sqrt{k^2 n_m^2 - |F|^2}\, e^{-iL\sqrt{k^2 n_m^2 - |F|^2}}$$
$$= A^T \sqrt{k^2 n_T^2 - |F|^2}\, e^{iL\sqrt{k^2 n_T^2 - |F|^2}} \tag{4.27}$$

$$\underbrace{\begin{bmatrix} e^{iL\sqrt{N_m}} & e^{-iL\sqrt{N_m}} \\ \sqrt{N_m}\, e^{iL\sqrt{N_m}} & -\sqrt{N_m}\, e^{-iL\sqrt{N_m}} \end{bmatrix}}_{M_3} \begin{bmatrix} A^m \\ B^m \end{bmatrix}$$
$$= \underbrace{\begin{bmatrix} e^{i\sqrt{N_T}L} & e^{-i\sqrt{N_T}L} \\ \sqrt{N_T}\, e^{i\sqrt{N_T}L} & e^{-i\sqrt{N_T}L} \end{bmatrix}}_{M_4} \begin{bmatrix} A^T \\ 0 \end{bmatrix} \tag{4.28}$$

where $N_T = k^2 n_T^2 - |F|^2$ and

At $z = -z_0$

$$B^B e^{iz_0\sqrt{k^2 n_b^2 - |F|^2}} = A^b e^{-iz_0\sqrt{k^2 n_b^2 - |F|^2}} + B^b e^{iz_0\sqrt{k^2 n_b^2 - |F|^2}} \tag{4.29}$$

We need to use the jump condition, which is the second one in equation (4.18) to obtain

$$A^b \sqrt{k^2 n_b^2 - |F|^2}\, e^{-iz_0\sqrt{k^2 n_b^2 - |F|^2}} - B^b \sqrt{k^2 n_b^2 - |F|^2}\, e^{iz_0\sqrt{k^2 n_b^2 - |F|^2}}$$
$$= -B^B \sqrt{k^2 n_b^2 - |F|^2}\, e^{iz_0\sqrt{k^2 n_b^2 - |F|^2}} + 1 \tag{4.30}$$

$$\underbrace{\begin{bmatrix} e^{-iz_0\sqrt{N_b}} & e^{iz_0\sqrt{N_b}} \\ \sqrt{N_b}\,e^{-iz_0\sqrt{N_b}} & -\sqrt{N_b}\,e^{iz_0\sqrt{N_b}} \end{bmatrix}}_{M_5} \begin{bmatrix} A^b \\ B^b \end{bmatrix}$$

$$= \underbrace{\begin{bmatrix} e^{iz_0\sqrt{N_b}} & e^{-iz_0\sqrt{N_b}} \\ -\sqrt{N_b}\,e^{iz_0\sqrt{N_b}} & e^{-iz_0\sqrt{N_b}} \end{bmatrix}}_{M_6} \begin{bmatrix} B^B \\ 0 \end{bmatrix} + \begin{bmatrix} 0 \\ 1 \end{bmatrix}$$

(4.31)

where $N_b = k^2 n_b^2 - |F|^2$. Now we can get the solution for the coefficient of the Green's function. Let's write our results in the simplified form

$$M_1 \begin{bmatrix} A^b \\ B^b \end{bmatrix} = M_2 \begin{bmatrix} A^m \\ B^m \end{bmatrix} \tag{4.32}$$

$$M_3 \begin{bmatrix} A^m \\ B^m \end{bmatrix} = M_4 \begin{bmatrix} A^T \\ 0 \end{bmatrix} \tag{4.33}$$

$$M_5 \begin{bmatrix} A^b \\ B^b \end{bmatrix} = M_6 \begin{bmatrix} B^B \\ 0 \end{bmatrix} + \begin{bmatrix} 0 \\ 1 \end{bmatrix} \tag{4.34}$$

where the reflection and the transmission amplitudes can be expressed in terms of the amplitude of the incident wave A^b

$$\begin{bmatrix} A^b \\ B^b \end{bmatrix} = \underbrace{M_1^{-1} M_2 M_3^{-1} M_4}_{\beta} \begin{bmatrix} A^T \\ 0 \end{bmatrix} \tag{4.35}$$

$$A^b = \beta_{1,1} A^T \qquad B^b = \beta_{2,1} A^T \tag{4.36}$$

$$B^b = \frac{\beta_{2,1}}{\beta_{1,1}} A^b \qquad A^T = \frac{A^b}{\beta_{1,1}} \tag{4.37}$$

Doing some algebra, we get the reflectance and the reflection coefficient $R = r*r$.

where

$$r = \frac{B^b}{A^b} = \frac{\left(\sqrt{N_T}+\sqrt{N_m}\right)\left(\sqrt{N_b}-\sqrt{N_m}\right)+\left(-\sqrt{N_T}+\sqrt{N_m}\right)\left(\sqrt{N_b}+\sqrt{N_m}\right)e^{i2L\sqrt{N_m}}}{\left(\sqrt{N_T}+\sqrt{N_m}\right)\left(\sqrt{N_b}+\sqrt{N_m}\right)+\left(-\sqrt{N_B}+\sqrt{N_m}\right)\left(\sqrt{N_T}-\sqrt{N_m}\right)e^{i2L\sqrt{N_m}}} \tag{4.38}$$

By the same technique, we can obtain the transmittance and the transmission coefficient $T = t^*t$.

where

$$t = \frac{A^T}{A^b} = \frac{4\sqrt{N_b}\sqrt{N_m}e^{-iL\sqrt{N_T}}}{\left(\sqrt{N_b}+\sqrt{N_m}\right)\left(\sqrt{N_T}+\sqrt{N_m}\right)e^{-iL\sqrt{N_m}}+\left(\sqrt{N_b}-\sqrt{N_m}\right)\left(-\sqrt{N_T}+\sqrt{N_m}\right)e^{iL\sqrt{N_m}}}$$

(4.39)

We also get the other coefficients inside the medium

$$\begin{bmatrix} A^m \\ B^m \end{bmatrix} = \underbrace{M_3^{-1}M_4}_{P}\begin{bmatrix} A^T \\ 0 \end{bmatrix}$$

(4.40)

$$A^m = \mathrm{P}_{1,1}A^T = \frac{\mathrm{P}_{1,1}}{\beta_{1,1}}A^b \quad B^m = \mathrm{P}_{2,1}A^T = \frac{\mathrm{P}_{2,1}}{\beta_{1,1}}A^b$$

(4.41)

$$\frac{A^m}{A^b} = \frac{2\sqrt{N_b}\left(\sqrt{N_m}+\sqrt{N_T}\right)}{\left(\sqrt{N_T}+\sqrt{N_m}\right)\left(\sqrt{N_b}+\sqrt{N_m}\right)+\left(-\sqrt{N_b}+\sqrt{N_m}\right)\left(\sqrt{N_T}-\sqrt{N_m}\right)e^{i2L\sqrt{N_m}}}$$

(4.42)

$$\frac{B^m}{A^b} = \frac{2\sqrt{N_b}\left(\sqrt{N_m}-\sqrt{N_T}\right)}{\left(\sqrt{N_T}+\sqrt{N_m}\right)\left(\sqrt{N_b}+\sqrt{N_m}\right)+\left(-\sqrt{N_b}+\sqrt{N_m}\right)\left(\sqrt{N_T}-\sqrt{N_m}\right)e^{i2L\sqrt{N_m}}}$$

(4.43)

At the source, we obtain

$$\begin{bmatrix} B^B \\ 0 \end{bmatrix} = M_6^{-1}\left\{\left(M_5M_1^{-1}M_2M_3^{-1}M_4\right)\begin{bmatrix} A^T \\ 0 \end{bmatrix} - \begin{bmatrix} 0 \\ 1 \end{bmatrix}\right\}$$

(4.44)

and if we let

$$X = M_6^{-1}M_5M_1^{-1}M_2M_3^{-1}M_4$$

(4.45)

$$S = M_6^{-1}\begin{bmatrix} 0 \\ 1 \end{bmatrix} = \begin{bmatrix} -\dfrac{1}{e^{iz_0\sqrt{N_b}}(1+\sqrt{N_b})} \\ \dfrac{1}{e^{-iz_0\sqrt{N_b}}(1+\sqrt{N_b})} \end{bmatrix}$$

(4.46)

34

then equation (4.44) becomes

$$\begin{bmatrix} B^B \\ 0 \end{bmatrix} = X \begin{bmatrix} A^T \\ 0 \end{bmatrix} - S \tag{4.47}$$

where $B^B = X_{1,1}A^T - S_{1,1} = \left(\dfrac{X_{1,1}}{\beta_{1,1}}\right)A^b - S_{1,1}$ and $0 = X_{2,1}A^T - S_{2,1}$ (4.48)

We know that the refractive indexes outside of the medium are the same: $N_b = N_T = N$.
What we need for our simulation are the amplitudes of the incident wave (A^b), the reflected wave (B^b), and the transmitted wave (A^T).

$$A^b = \frac{e^{iz_0\sqrt{N}}}{2\sqrt{N}} \tag{4.49}$$

$$B^b = r * A^b = \frac{(N - N_m) + (N_m - N)e^{i2L\sqrt{N_m}}}{\left(\sqrt{N_m} + \sqrt{N}\right)^2 - \left(\sqrt{N_m} - \sqrt{N}\right)^2 e^{i2L\sqrt{N_m}}} \frac{e^{iz_0\sqrt{N}}}{2\sqrt{N}} \tag{4.50}$$

$$A^T = t * A^b = \frac{4\sqrt{N}\sqrt{N_m}\, e^{-iL\sqrt{N}}}{\left(\sqrt{N} + \sqrt{N_m}\right)^2 e^{-iL\sqrt{N_m}} - \left(\sqrt{N_m} - \sqrt{N}\right)^2 e^{iL\sqrt{N_m}}} \frac{e^{iz_0\sqrt{N}}}{2\sqrt{N}} \tag{4.51}$$

Since the free space Green's function is a solution of the Helmholtz equation and satisfies the radiation condition at infinity, this should be the solution in that region. The following are the Green's functions we are interested in :

For the region $-z_0 < z < 0$,

$$G(v_x, v_y, z, r_0) = \begin{cases} \dfrac{e^{iz_0\sqrt{N}}}{2\sqrt{N}} e^{iz\sqrt{k^2 - |F|^2}} & right\ going \\[4mm] \dfrac{(N - N_m) + (N_m - N)e^{i2L\sqrt{N_m}}}{\left(\sqrt{N_m} + \sqrt{N}\right)^2 - \left(\sqrt{N_m} - \sqrt{N}\right)^2 e^{i2L\sqrt{N_m}}} \dfrac{e^{iz_0\sqrt{N}}}{2\sqrt{N}} e^{-iz\sqrt{k^2 - |F|^2}} & left\ going \end{cases} \tag{4.52}$$

For the region $z > L$,

35

$$G(v_x, v_y, z, r_0) = \frac{4\sqrt{N}\sqrt{N_m}\, e^{-iL\sqrt{N}}}{\left(\sqrt{N} + \sqrt{N_m}\right)^2 e^{-iL\sqrt{N_m}} - \left(\sqrt{N_m} - \sqrt{N}\right)^2 e^{iL\sqrt{N_m}}} \frac{e^{iz_0\sqrt{N}}}{2\sqrt{N}} e^{iz\sqrt{k^2 - |F|^2}} \quad right\ going$$

$$(4.53)$$

We can also get the coefficient A^m and B^m by solving this

$$\begin{bmatrix} A^m \\ B^m \end{bmatrix} = M_2^{-1} M_1 \begin{bmatrix} A^b \\ B^b \end{bmatrix}$$

$$(4.54)$$

For the region $0 < z < L$, we get these coefficients

$$A^m = \frac{e^{iz_0\sqrt{N}}}{2\sqrt{N}} \times \frac{2\sqrt{N}\left(\sqrt{N} + \sqrt{N_m}\right)}{\left(\sqrt{N} + \sqrt{N_m}\right)^2 - \left(\sqrt{N_m} - \sqrt{N}\right)^2 e^{i2L\sqrt{N_m}}}$$

$$(4.55)$$

$$B^m = \frac{e^{iz_0\sqrt{N}}}{2\sqrt{N}} \times \frac{2\sqrt{N}\left(\sqrt{N_m} - \sqrt{N}\right)e^{i2L\sqrt{N_m}}}{\left(\sqrt{N} + \sqrt{N_m}\right)^2 - \left(\sqrt{N_m} - \sqrt{N}\right)^2 e^{i2L\sqrt{N_m}}}$$

$$(4.56)$$

Finally, we obtain the Green's function in the media

$$G(v_x, v_y, z, r_0) = A^m e^{iz\sqrt{n^2 k^2 - |F|^2}} \quad right\ going\ wave$$

$$(4.57)$$

$$G(v_x, v_y, z, r_0) = B^m e^{-iz\sqrt{n^2 k^2 - |F|^2}} \quad left\ going\ wave$$

$$(4.58)$$

V.   THE ANGULAR SPECTRUM

A.   TRANSFORM SPHERICAL WAVES

The angular spectrum method is a technique for modeling the propagation of a wave field. This method involves expanding a complex wave field into a summation of many plane waves. As the spherical waves propagate through a wall, they are appropriately described by a planer expansion, because waves propagate in all directions spherically, and the boundary is plane. We have to transform the spherical waves to plane waves, since the reflected wave from a plane media with a spherical wave is also spherical [21]. To obtain the angular spectrum $g(x, y, z, r_0)$ we need to take the Inverse Fourier Transform of the right going wave in the region $-z_0 < z < 0$ in equation (4.52). We obtain

$$g(x, y, z, r_0) \equiv \int_{-\infty}^{\infty} \int_{-\infty}^{\infty} G(v_x, v_y, z, r_0) e^{i(2\pi v_x x + 2\pi v_y y)} dv_x dv_y \qquad (5.1)$$

In this region, the refractive index is $n = 1$, and equation (5.1) becomes

$$g(x, y, z, r_0) = \int_{-\infty}^{\infty} \int_{-\infty}^{\infty} \frac{e^{iz_0\sqrt{k^2-(2\pi v_x)^2-(2\pi v_y)^2}}}{2\sqrt{k^2-(2\pi v_x)^2-(2\pi v_y)^2}} e^{iz\sqrt{k^2-(2\pi v_x)^2-(2\pi v_y)^2}} e^{i2\pi(v_x x+v_y y)} dv_x dv_y \quad (5.2)$$

$$g(x, y, z, r_0) = \int_{-\infty}^{\infty} \int_{-\infty}^{\infty} \frac{e^{ik(z_0+z)\sqrt{1-(2\pi v_x/k)^2-(2\pi v_y/k)^2}}}{2k\sqrt{1-(2\pi v_x/k)^2-(2\pi v_y/k)^2}} e^{i(2\pi v_x x+2\pi v_y y)} dv_x dv_y \qquad (5.3)$$

Let's suppose a wave vector $\bar{k}$ has magnitude $\dfrac{2\pi}{\lambda}$ and direction cosines (α, β, γ), (See Figure 9) then $\bar{k}$ is expressed as

$$\bar{k} = k_x \hat{x} + k_y \hat{y} + k_z \hat{z} = k(\alpha \hat{x} + \beta \hat{y} + \gamma \hat{z}) \qquad (5.4)$$

$$= \frac{2\pi}{\lambda}(\alpha \hat{x} + \beta \hat{y} + \sqrt{1-\alpha^2-\beta^2}\,\hat{z}) \qquad (5.5)$$

since direction cosines are $\alpha^2 + \beta^2 + \gamma^2 = 1$ where

$$k_x = \overline{k} \cdot \hat{x} = k\alpha$$
$$k_y = \overline{k} \cdot \hat{y} = k\beta$$
$$k_z = \overline{k} \cdot \hat{z} = k\gamma$$

Then we can get the following identities

$$k_x = k\alpha, \quad k_y = k\beta \quad \Rightarrow \quad \alpha = \frac{2\pi v_x}{k}, \quad \beta = \frac{2\pi v_y}{k}$$

$$d\alpha = \frac{2\pi df_x}{k}, \quad d\beta = \frac{2\pi df_y}{k}$$

Using these identities, equation (5.3) becomes

$$g(\alpha, \beta, z, r_0) = \int_{-\infty}^{\infty} \int_{-\infty}^{\infty} \frac{e^{ik(z_0+z)\sqrt{1-\alpha^2-\beta^2}}}{2k\sqrt{1-\alpha^2-\beta^2}} e^{ik(\alpha x+\beta y)} \left(\frac{k}{2\pi}\right) d\alpha \left(\frac{k}{2\pi}\right) d\beta$$

$$= \left(\frac{k}{8\pi^2}\right) \int_{-\infty}^{\infty} \int_{-\infty}^{\infty} \frac{e^{ik\gamma(z_0+z)} e^{ik(\alpha x+\beta y)}}{\gamma} d\alpha d\beta \tag{5.6}$$

From H. Weyl's expansion of the spherical waves into planar waves [22]
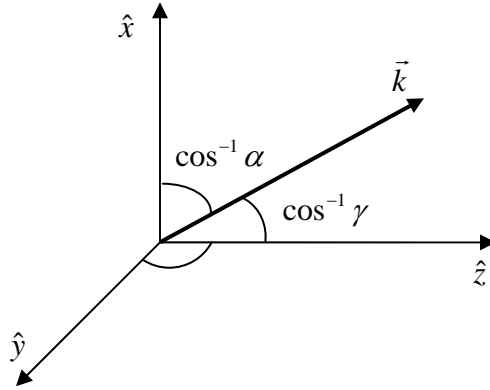

Figure 9.   The wave vector $\vec{k}$

$$\frac{e^{ik|r-r'|}}{|r-r'|} = \frac{i}{2\pi} \int_{-\infty}^{\infty} \int_{-\infty}^{\infty} \frac{1}{\gamma} e^{ik[\alpha(x-x')+\beta(y-y')+\gamma(z-z')]} d\alpha d\beta \qquad (5.7)$$

where $r = x\hat{x} + y\hat{y} + z\hat{z}, \quad r' = x'\hat{x} + y'\hat{y} + z'\hat{z}$

Substituting equation (5.6) into equation (5.7), we get

$$g(x,y,z,r_0) = \frac{k}{i4\pi} \frac{e^{ik|r-r_0|}}{|r-r_0|} \qquad (5.8)$$

and applying the far-field approximation to equation (5.8), we obtain

$$g(x,y,z,r_0) \simeq \frac{ke^{ikr}}{i4\pi r} e^{-ik\hat{r}\cdot r_0} \qquad (5.9)$$

B.   REFLECTIVITY OF MEDIA

In the previous chapter, we obtained planer expansions of Green's functions. To calculate the reflectivity on the surface, we need to employ spherical coordinates. In equation (4.52), we see the reflectivity (R) from left going waves as

$$R = \frac{(N - N_m) + (N_m - N)e^{i2L\sqrt{N_m}}}{\left(\sqrt{N_m} + \sqrt{N}\right)^2 - \left(\sqrt{N_m} - \sqrt{N}\right)^2 e^{i2L\sqrt{N_m}}} \qquad (5.10)$$

where,

$$\sqrt{N_m} = \sqrt{n_m^2 k^2 - (2\pi v_x)^2 - (2\pi v_y)^2} \quad , \quad \sqrt{N} = \sqrt{k^2 - (2\pi v_x)^2 - (2\pi v_y)^2} \qquad (5.11)$$

The spherical expansion of the reflected wave can be obtained by converting R into spherical coordinates. Using the relationship in equation (5.4) and the spherical coordinate representation, we obtain

$$2\pi v_x = k \sin\theta \cos\phi, \ 2\pi v_y = k \sin\theta \cos\phi, \ 2\pi v_z = k \cos\theta \qquad (5.12)$$

Substituting equation (5.12) into equation (5.11), we get

$$\sqrt{N_m} = k\sqrt{n_m^2 - \sin^2\theta} \ , \ \sqrt{N} = k\sqrt{1 - \sin^2\theta} = k\cos\theta \qquad (5.13)$$

And inserting these results into equation (5.10), we get the reflectivity as

$$R(\theta) = \frac{(1 - n_m^2) + (n_m^2 - 1)e^{i2kL\sqrt{n^2 - \sin^2\theta}}}{\left(\sqrt{n_m^2 - \sin^2\theta} + \sqrt{1 - \sin^2\theta}\right)^2 - \left(\sqrt{n_m^2 - \sin^2\theta} - \sqrt{1 - \sin^2\theta}\right)^2 e^{i2kL\sqrt{n_m^2 - \sin^2\theta}}} \qquad (5.14)$$

$$= \frac{(1 - n_m^2) + (n_m^2 - 1)e^{i2kL\sqrt{n_m^2 - \sin^2\theta}}}{\left(\sqrt{n_m^2 - \sin^2\theta} + \cos\theta\right)^2 - \left(\sqrt{n_m^2 - \sin^2\theta} - \cos\theta\right)^2 e^{i2kL\sqrt{n_m^2 - \sin^2\theta}}} \qquad (5.15)$$

C.   EVANESCENT WAVES

The electric field does not abruptly vanish at the boundary, because the phase difference between the incident and reflected waves prevents the complete destructive interference required to eliminate the transmitted wave. The transmitted field that extends beyond the boundary of the dielectric, when a wave is totally internally reflected, is known as the evanescent wave [19].

If we choose a coordinate system in which the boundary lies in the $x - y$ plane and $\vec{k}$ lies in the $x - z$ plane and suppose we have a transmitted wave of the form

$$\vec{E}_t = \vec{E}_{t,0}e^{i(\vec{k}_t \cdot \vec{r} - \omega t)} \qquad (5.16)$$

then, we can rewrite this with Snell's law as

$$\vec{k}_t \cdot \vec{r} = k_t x \sin\theta_t + k_t z \cos\theta_t \qquad (5.17)$$

$$= k_t \left(\frac{x\sin\theta_i}{n} + iz\sqrt{\frac{\sin\theta_i}{n^2} - 1} \right) \qquad (5.18)$$

Substituting equation (5.18) into equation (5.16), we get the transmitted field

$$E_t(\vec{r}, t) = \vec{E}_{t,0}e^{-k''z}e^{i(k'x - \omega t)} \qquad (5.19)$$

40

where k'' is a constant and $k' = k_t \sin\theta_t$. This wave propagates along the boundary with propagation constant k', diminishing exponentially with constant k''.

Let's look at the region $-z_0 < z < L$ and examine how much the wave evanesces. We need equation (4.52) and equation (4.57) for the reflection and transmission.

$$g(x, y, z, r_0) = \tilde{A}(v_x, v_y) e^{-i(z+z_0)\sqrt{k^2 - (2\pi v_x)^2 - (2\pi v_y)^2}} e^{i(2\pi v_x x + 2\pi v_y y)} \tag{5.20}$$

$$g(x, y, z, r_0) = \tilde{A}'(v_x, v_y) e^{i(z+z_0)\sqrt{n^2 k^2 - (2\pi v_x)^2 - (2\pi v_y)^2}} e^{i(2\pi v_x x + 2\pi v_y y)} \tag{5.21}$$

For the reflected wave in equation (5.20), there is an angle of incidence that results in a transmission angle that is parallel to the surface. If the incident angle increases over the critical angle, the transmitted wave will evanesce. In the region $z < 0$, the intensity of reflection wave is

$$I = g^* g = A^* A e^{2(z+z_0)\sqrt{(2\pi v_x x)^2 - (2\pi v_y y)^2 - k^2}} \tag{5.22}$$

As z goes negative, the intensity becomes smaller, so the evanescing wave will be much smaller. Therefore in this model system, we will ignore the evanescent waves as unimportant.
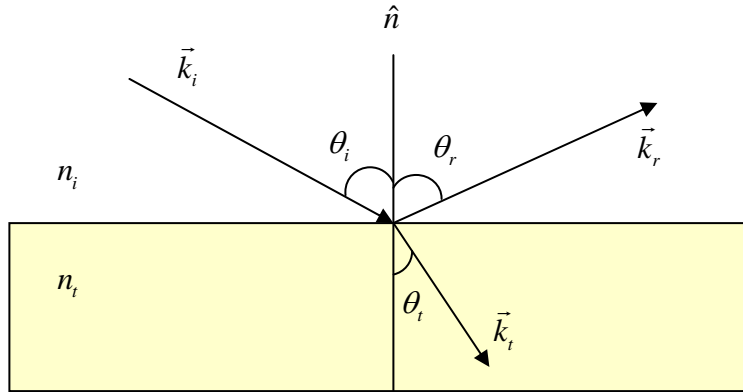
Figure 10.   The wave vector $\vec{k}_i$, $\vec{k}_r$ and $\vec{k}_t$

41
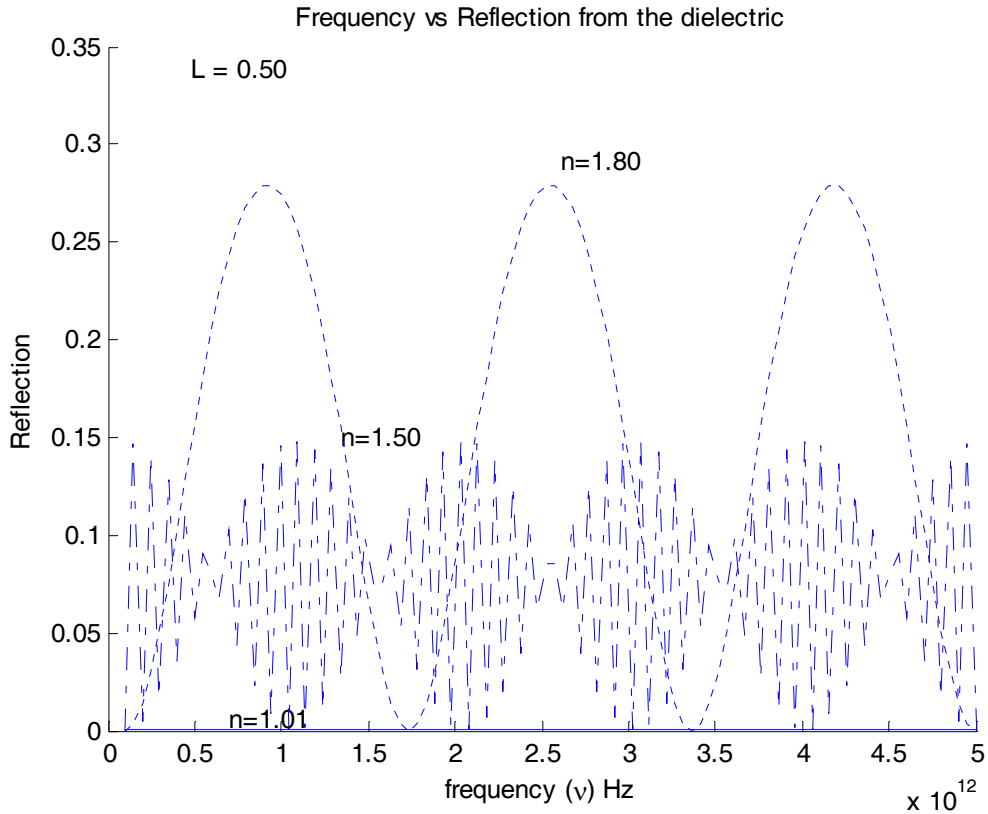
Figure 11.   Reflection (polystyrene, quartz, glass)

D.   MATERIAL ANALYSIS

Typical materials of common walls are wood, tile, and concrete. These materials have their own refractivity defined by the index of refraction

$$n = \frac{c}{v} = \frac{\sin \theta_i}{\sin \theta_r} \qquad (5.23)$$

The refractive indexes of materials depend on the frequency with which it is measured. Unfortunately, indices of refraction in the terahertz region have not been well tabulated.

Not all light striking a transparent material is refracted as shown in Figure 10 [23]. The reflectance, R is related to the index of refraction by

$$R = \left(\frac{n_{k+1} - n_k}{n_{k+1} + n_k} \right)^2 \qquad (5.24)$$

(when the incident angle $\theta_i = 0$).

From equation (5.24), we can predict that the higher-n materials are the more refractive. In this section, we will analyze materials using MATLAB simulations based on equation (5.15) and find appropriate frequencies that can penetrate wall materials without much loss and with good reflection of objects. For this simulation, we assume that we are using plane waves and normal incidence.

One of the most attractive advantages about terahertz frequencies is their ability to penetrate many common materials. But the terahertz pulse can't penetrate materials with high water content, so we assume the materials used in this simulation are pre-dried. Table II shows index of refraction for common materials in terahertz frequency [4, 8].

Figure 11 shows that as we increase the index of refraction, the reflection becomes large. In Figure 12, we used refractive indexes of common wall materials. In the case of tile, rock, and sand the average reflection is quite high. But if we look at this figure closely, we can find the frequencies that have low reflection from these materials. These frequencies are at about 0.94THz, 1.44THz, etc. and can be used for Through-the-Wall Imaging.

Polystyrene foam	1.01
Ochroma pyramidale	1.08
Lophira lata (wood)	1.49
Skin	1.4
Body fluid	3.9
Sand	1.67
Glass	1.8
Quartz	1.5
Tile	1.6
Stone	1.6

Table 2.   Index of refraction for common materials.

Figure 12.   Reflection (lophira, tile, sand)
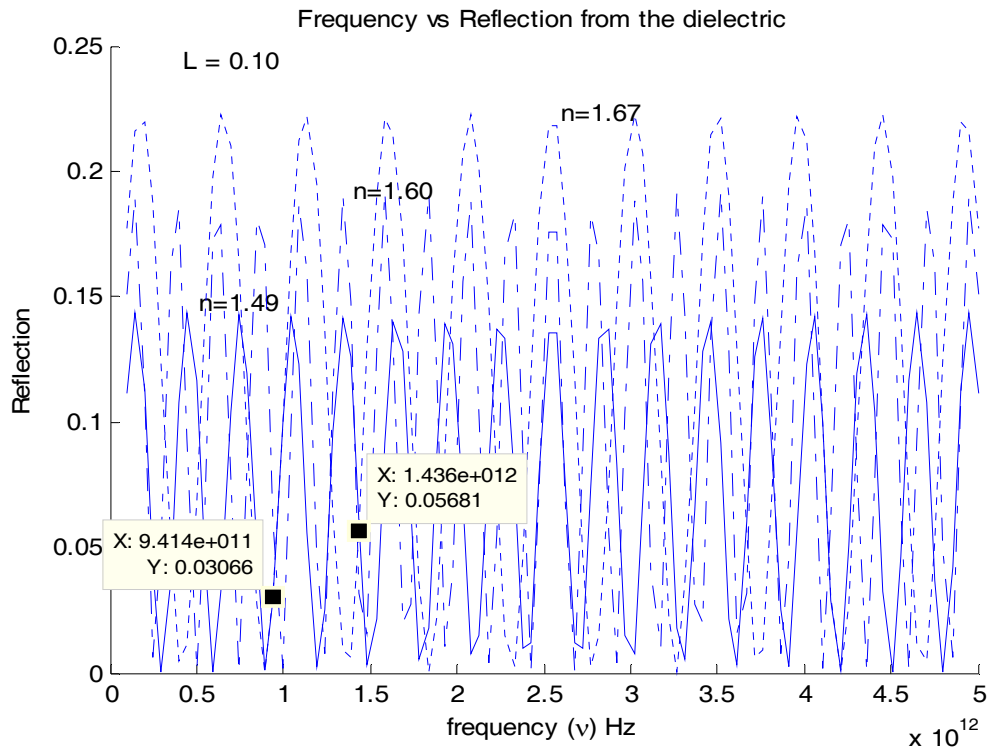
We also used the index of refraction of human skin and body fluid. Figure 13 illustrates the reflection from body fluid is very high at frequency 0.94THz. Consequently, if we choose 0.94THz frequency for Through-the-Wall Imaging, we will get more data from the human body and get a good image.
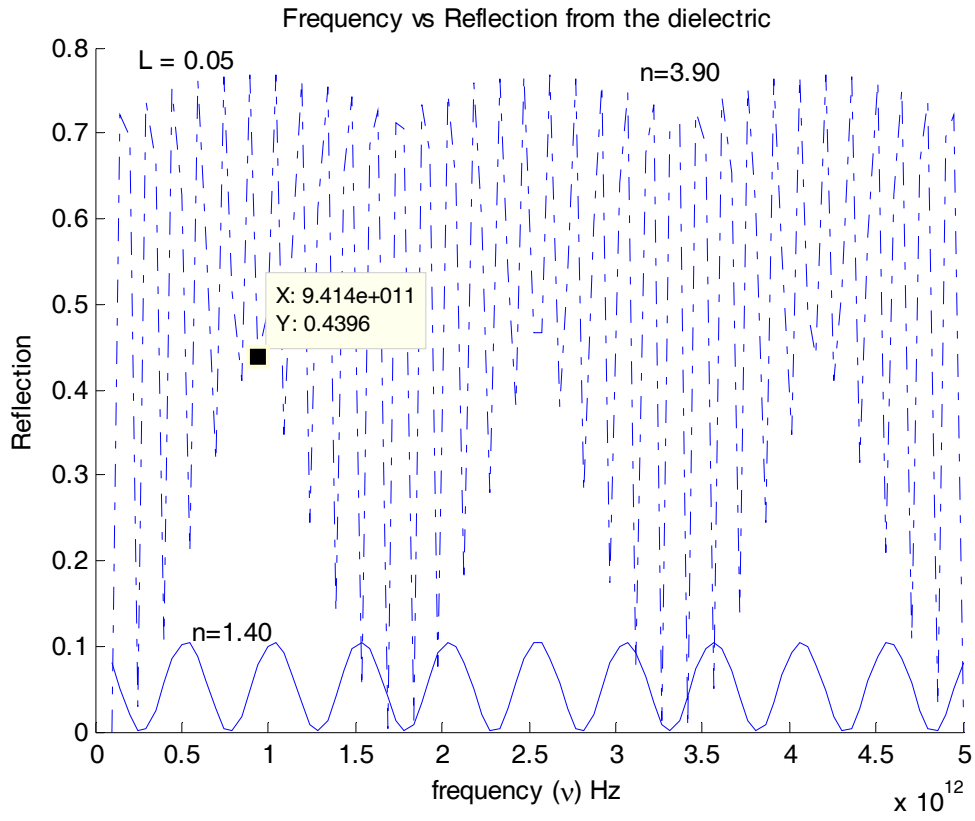

Figure 13.   Reflection (body fluid, skin)

THIS PAGE INTENTIONALLY LEFT BLANK

VI.   INTEGRAL EQUATION

A.   WAVE PROPAGATION EQUATION

In this thesis we are assuming that the complex dielectric constant and magnetic permeability vary slowly over a wavelength of the electromagnetic wave, and we are neglecting polarization effects. Then we can write the Helmholtz equation as

$$\nabla^2 E(\mathbf{r}) + k^2 n_{obj}^2(\mathbf{r})E(\mathbf{r}) = 0 \tag{6.1}$$

If we add $k^2 E(\mathbf{r})$ on both sides we get

$$\nabla^2 E(\mathbf{r}) + k^2 E(\mathbf{r}) = -\underbrace{k^2 (n_{obj}(\mathbf{r})^2 - 1)}_{O(\mathbf{r})} E(\mathbf{r}) \tag{6.2}$$

where $O(\mathbf{r})$ is the target's object function and is denoted by

$$O(\mathbf{r}) = k^2 (n_{obj}^2 - 1) \, . \tag{6.3}$$

Then the total electric field $E(\mathbf{r})$ solution to equation (6.2) is

$$E(\mathbf{r}) = E_{inc}(\mathbf{r}) + \int_V g(\mathbf{r} - \mathbf{r_0})O(\mathbf{r_0})E(\mathbf{r_0})d\mathbf{r_0} \tag{6.4}$$

where g is the Green's function of the Helmholtz equation and is the solution of the differential equation

$$(\nabla^2 + k^2)g(\mathbf{r} - \mathbf{r_0}) = -\delta(\mathbf{r} - \mathbf{r_0}) \tag{6.5}$$

where $\delta(\mathbf{r} - \mathbf{r_0})$ is the Dirac delta function. In our model system, the Green's function varies as the observation point changes. From the previous chapter, we found Green's functions in the spatial frequency domain as Eq.(4.52), Eq.(4.53), Eq.(4.57), and Eq.(4.58). So in order to get $g(\mathbf{r} - \mathbf{r_0})$, we have to transform these Green's functions using the Inverse Fourier Transform as

$$g(\mathbf{r} - \mathbf{r_0}) = \iiint G(v_x, v_y, z, r_0)e^{i2\pi(v_x x + v_y y)}dv_x dv_y \tag{6.6}$$

47
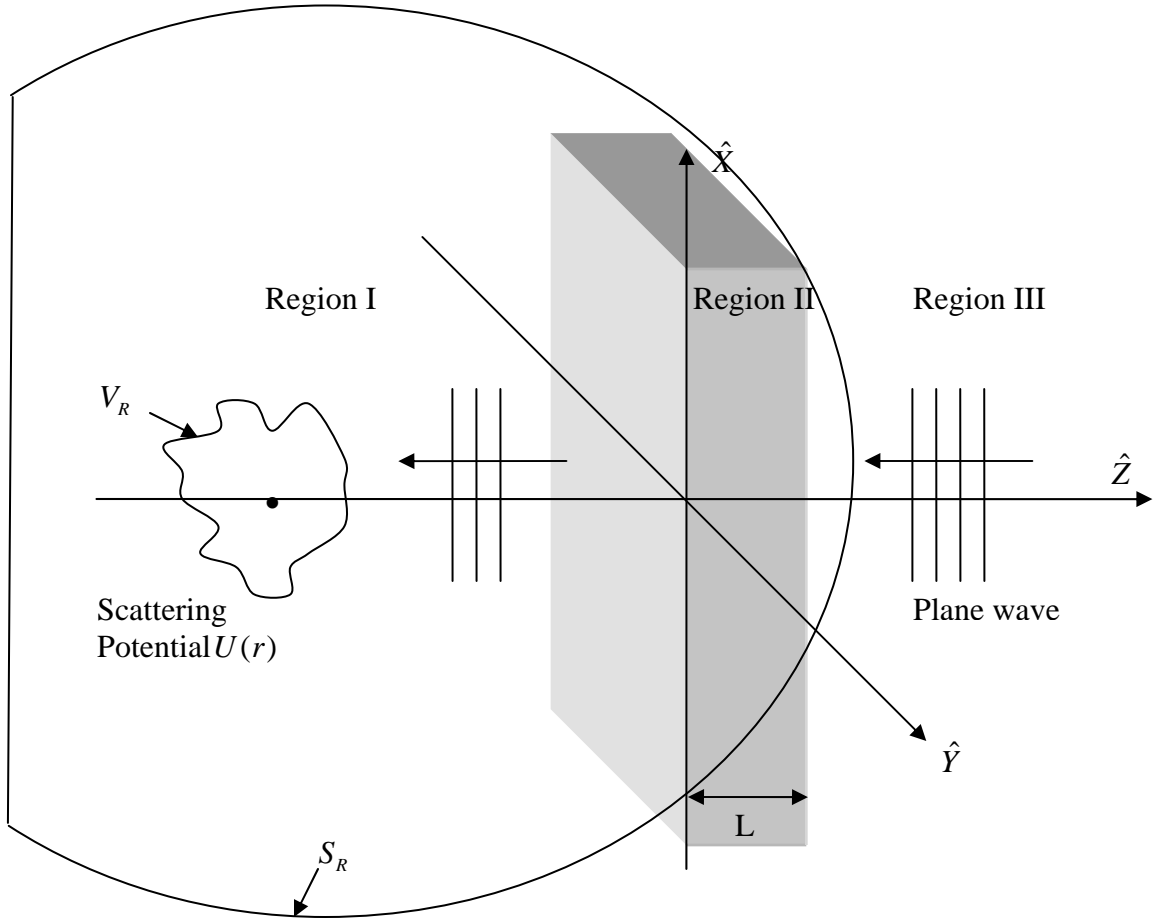
Figure 14.   Illustration of a scattering of volume V_R bounded by surface S_R

We denote each Green's function by their domain as

$$
\begin{aligned}
g_I(\mathbf{r} - \mathbf{r_0}) &\quad for \quad z < 0 \\
g_{II}(\mathbf{r} - \mathbf{r_0}) &\quad for \quad 0 \le z \le L \\
g_{III}(\mathbf{r} - \mathbf{r_0}) &\quad for \quad L < z
\end{aligned}
$$

and we will use $g_{III}(\mathbf{r} - \mathbf{r_0})$ for our model system in the following section.

B.   THE FIRST BORN APPROXIMATION

The Born approximation is perhaps the simplest and most widely used EM scattering approximation. It is based on the assumption that scattered electric fields inside

scatterers are negligible compared to the normal/background electric fields. Hence the second term on the right hand side of equation (6.4) is small in comparison to the first term within the integral. In the integrand can approximate

$$E(r) \approx E_{inc}(\mathbf{r}) \tag{6.7}$$

Therefore the total electric field in equation (6.4) is calculated as

$$E(\mathbf{r}) = E_{inc}(\mathbf{r}) + \int_V g(\mathbf{r} - \mathbf{r_0})O(\mathbf{r_0})E_{inc}(\mathbf{r_0})d^3\mathbf{r_0} \tag{6.8}$$

Consequently, the scattered field, E_s, can be identified with

$$E_s = \int_V g(\mathbf{r} - \mathbf{r_0})O(\mathbf{r_0})E_{inc}(\mathbf{r_0})d^3\mathbf{r_0} \tag{6.9}$$

C.   THE FIRST RYTOV APPROXIMATION

The Rytov approximation assumes that the incident wave perturbation caused by the target can be described by a change of phase in the reference wave. The Rytov approximation is obtained by representing the total field as a complex phase [22]

$$E(\mathbf{r}) = e^{\phi(\mathbf{r})} \tag{6.10}$$

We consider the scattering of a scalar wave in an inhomogeneous medium. The field satisfies the reduced wave equation

$$\nabla^2 E(\mathbf{r}) + k^2 E(\mathbf{r}) = 0 \tag{6.11}$$

Substituting equation (6.10) into equation (6.11), we get

$$\nabla^2 e^{\phi(\mathbf{r})} + k^2 e^{\phi(\mathbf{r})} = 0 \tag{6.12}$$

Using the identity

$$\nabla^2 e^{\phi(\mathbf{r})} = \nabla^2 \phi e^{\phi(\mathbf{r})} + (\nabla\phi)(\nabla\phi)e^{\phi(\mathbf{r})} \tag{6.13}$$

we substitute equation (6.13) into equation (6.12) and divide by $e^{\phi(\mathbf{r})}$ on both sides and get the following Riccati equation

$$\nabla^2 \phi + (\nabla\phi)(\nabla\phi) + k^2 = 0 \tag{6.14}$$

We denote the refractive index as

$$k(\mathbf{r}) = k_0 n(\mathbf{r}) = k_0 (1 + n\delta(\mathbf{r})) \tag{6.15}$$

The zero perturbation field for $n(r) = 1$ can be written as $E_i(\mathbf{r}) = e^{\phi_i(\mathbf{r})}$, and its phase will satisfy equation (6.14)

$$\nabla^2 \phi_i + (\nabla \phi_i)^2 + k_0^2 = 0 \tag{6.16}$$

We can express the total complex phase, ϕ, as the sum of the incident phase ϕ_i and the scattered complex phase ϕ_s

$$\phi = \phi_i + \phi_s \tag{6.17}$$

Now substitute equation (6.17) into equation (6.14)

$$\nabla^2(\phi_i + \phi_s) + (\nabla(\phi_i + \phi_s))^2 + k^2 = 0 \tag{6.18}$$

Expanding this equation

$$\nabla^2 \phi_i + \nabla^2 \phi_s + (\nabla \phi_i)^2 + (\nabla \phi_s)^2 + 2(\nabla \phi_i)(\nabla \phi_s) + k^2 = 0 \tag{6.19}$$

and subtract equation (6.16) from equation (6.19), we get

$$\nabla^2 \phi_s + 2(\nabla \phi_i)(\nabla \phi_s) + (k^2 - k_0^2) = -(\nabla \phi_s)^2 \tag{6.20}$$

$$\nabla^2 \phi_s + 2(\nabla \phi_i)(\nabla \phi_s) = -((\nabla \phi_s)^2 + k_0^2(n^2 - 1)) \tag{6.21}$$

Using the identity

$$\nabla^2(E_i \phi_s) = \phi_s \nabla^2 E_i + 2(\nabla E_i)(\nabla \phi_s) + E_i \nabla^2 \phi_s \tag{6.22}$$

and assuming a plane wave for the incident field, so that

$$E_i = A e^{i k_0 s \cdot r} = A e^{i \phi_i(r)} \tag{6.23}$$

then we find the following expression

$$\nabla^2 E_i = -k_0^2 E_i \quad \text{and} \quad \nabla E_i = E_i \nabla \phi_i \tag{6.24}$$

So equation (6.22) becomes

$$2E_i \nabla \phi_i \cdot \nabla \phi_s + E_i \nabla^2 \phi_s = \nabla^2(E_i \phi_s) + k_0^2 E_i \phi_s \tag{6.25}$$

Now substituting equation (6.25) into equation (6.21), we get

$$\nabla^2(E_i \phi_s) + k^2(E_i \phi_s) = -E_i \left\{ (\nabla \phi_s)^2 + k_0^2(n^2 - 1) \right\} \tag{6.26}$$

Solving this equation using the free space Green's function, we get

$$E_i(\mathbf{r})\phi_s(\mathbf{r}) = \int g(\mathbf{r} - \mathbf{r_0})E_i(\mathbf{r_0})\left\{ (\nabla \phi_s(\mathbf{r_0}))^2 + k_0^2(n^2(\mathbf{r_0}) - 1) \right\} d\mathbf{r_0} \tag{6.27}$$

$$\phi_s(\mathbf{r}) = \frac{1}{E_i(\mathbf{r})} \int g(\mathbf{r} - \mathbf{r_0})E_i(\mathbf{r_0})(\nabla \phi_s(\mathbf{r_0}))^2 d\mathbf{r_0} + \frac{1}{E_i(\mathbf{r})} \int g(\mathbf{r} - \mathbf{r_0})E_i(\mathbf{r_0})k_0^2(n^2(\mathbf{r_0}) - 1) d\mathbf{r_0} \tag{6.28}$$

50

By the Rytov approximation, the first term in equation (6.28) is very small, so equation (6.28) can be approximated as

$$\phi_s(\mathbf{r}) = \frac{1}{E_i(\mathbf{r})} \int g(\mathbf{r} - \mathbf{r_0}) E_i(\mathbf{r_0}) k_0^2 (n^2(\mathbf{r_0}) - 1) d\mathbf{r_0} \qquad (6.29)$$

If we denote the target object function $O(r)$ as

$$O(\mathbf{r}) = k_0^2 (n^2(\mathbf{r_0}) - 1) \qquad (6.30)$$

Then equation (6.29) becomes

$$\phi_s(\mathbf{r}) = \frac{1}{E_i(\mathbf{r})} \int g(\mathbf{r} - \mathbf{r_0}) E_i(\mathbf{r_0}) O(\mathbf{r_0}) d\mathbf{r_0} \qquad (6.31)$$

The corresponding solution for the total field is

$$E(\mathbf{r}) = E_i(\mathbf{r}) e^{\phi_s} \qquad (6.32)$$

But it is only valid when $(\nabla \phi_s)^2 \ \Box \ k_0^2 (n^2(\mathbf{r_0}) - 1)$

From equation (6.10), the total electric field is given

$$E(\mathbf{r}) = E_i(\mathbf{r}) + E_s(\mathbf{r}) = e^{\phi_0(\mathbf{r}) + \phi_s(\mathbf{r})} \qquad (6.33)$$

Rearranging this equation for the scattered field, $E_s(\mathbf{r})$, we get

$$E_s(\mathbf{r}) = E_i(\mathbf{r})(e^{\phi_s(\mathbf{r})} - 1) \qquad (6.34)$$

Substituting equation (6.31) into equation (6.34), finally we get the scattered field as

$$E_s(\mathbf{r}) = E_i(\mathbf{r_0}) \left[e^{\frac{1}{E_i(\mathbf{r})} \int g(\mathbf{r} - \mathbf{r_0}) E_i(\mathbf{r_0}) O(\mathbf{r_0}) d\mathbf{r_0}} - 1 \right] \qquad (6.35)$$

Note that when the argument of the exponential is small, then we can approximate

$$e^{\frac{1}{E_i(\mathbf{r})} \int g(\mathbf{r} - \mathbf{r_0}) E_i(\mathbf{r_0}) O(\mathbf{r_0}) d\mathbf{r_0}} \approx 1 + \frac{1}{E_i(\mathbf{r})} \int g(\mathbf{r} - \mathbf{r_0}) E_i(\mathbf{r_0}) O(\mathbf{r_0}) d\mathbf{r_0} \qquad (6.36)$$

and, in this case, the Rytov approximation reduces to the first Born approximation.

THIS PAGE INTENTIONALLY LEFT BLANK

VII. SIMULATION

A. RECONSTRUCTION ALGORITHM

For many reasons, it is very useful to convert functions in the time domain into functions in the frequency domain. The primary reason is that it gives us an easy way to solve difficult problems. For instance, when we meet the convolution integral in the time domain, we can express this as a simple multiplication integral in the frequency domain.

To apply the Rytov approximation for object reconstruction, we need to estimate the scattered field $E_s(\mathbf{r})$, which is denoted in equation (6.35). From equation (6.35) we have

$$E_i(\mathbf{r})\ln\left[\frac{E_s(\mathbf{r})}{E_i(\mathbf{r_0})}+1\right]=\int_{V_R}g(\mathbf{r}-\mathbf{r_0})E_i(\mathbf{r_0})O(\mathbf{r_0})d\mathbf{r_0} \tag{7.1}$$

Since a kernel is formed as a convolution between the Green's function, the scattering potential, and the incident electric field, we make a reconstruction algorithm in the frequency domain by Fourier Transform of the measurement data. The left term in equation (7.1) is our measurement data. If we denote this by $m(r)$, and then

$$m(r)=\int_{V_R}g(\mathbf{r}-\mathbf{r_0})E_i(\mathbf{r_0})O(\mathbf{r_0})d\mathbf{r_0} \tag{7.2}$$

We extend the volume integral to infinity and take 2D Fourier Transform by assuming receivers will be place at fixed points (x_i, y_i, z). Then equation (7.2) becomes

$$M(v_x, v_y)=G(v_x, v_y)X(v_x, v_y) \tag{7.3}$$

where,

$$X(v_x, v_y)=\int\int_{-\infty}^{\infty}E_i(x_0, y_0)O(x_0, y_0)e^{-i2\pi(v_x x+v_y y)}dxdy \tag{7.4}$$

By using equation (7.3) and applying equation (2.9) we can get $\overline{X}(v_x, v_y)$ as

$$\overline{X}(v_x, v_y) = \left\{ \left(G(v_x, v_y)^T G(v_x, v_y) \right)^{-1} G(v_x, v_y)^T \right\} M(v_x, v_y) \qquad (7.5)$$

Substituting equation (7.5) into equation (7.4), we can get the "best object" $\overline{O}(r_0)$ and taking the Inverse Fourier Transform of this as

$$\overline{O}(r_0) = \frac{1}{E_i(\mathbf{r_0})} \int\int_{-\infty}^{\infty} \left[\left\{ \left(G(v_x, v_y)^T G(v_x, v_y) \right)^{-1} G(v_x, v_y)^T \right\} M(v_x, v_y) \right] e^{i2\pi(v_x x + v_y y)} dx dy \quad (7.6)$$

Finally, we get the "best object" $\overline{O}(r_0)$ in the spatial domain. The incident wave $E_i(r) = Ae^{-ikz}$ becomes $E_i'(r) = tAe^{-ikz}$ after passing through a transparent media with transmittance t. The Green's function to be used in equation (7.6) is

$$G(v_x, v_y, z, r_0) = \frac{4\sqrt{N}\sqrt{N_m} e^{-iL\sqrt{N}}}{\left(\sqrt{N} + \sqrt{N_m} \right)^2 e^{-iL\sqrt{N_m}} - \left(\sqrt{N_m} - \sqrt{N} \right)^2 e^{iL\sqrt{N_m}}} \frac{e^{iz_0\sqrt{N}}}{2\sqrt{N}} e^{iz\sqrt{k^2 - |F|^2}} \quad (7.7)$$

B. MATLAB CODE IMPLEMENTATION

The total field at the receivers will be composed of the incident field from transmitters, the reflected field from the wall, the scattered field from the target, and the evanescing field. In the previous chapter, we showed the evanescent field is negligible in comparison with the incident field.

For our image processing, we are only interested in the scattered field data and use equation (6.35) and equation (7.6) to create scattered field images. Due to the limitation of computer ability, we are restricted in the number of scattering points to the sampling frequency, and bandwidth to be examined.
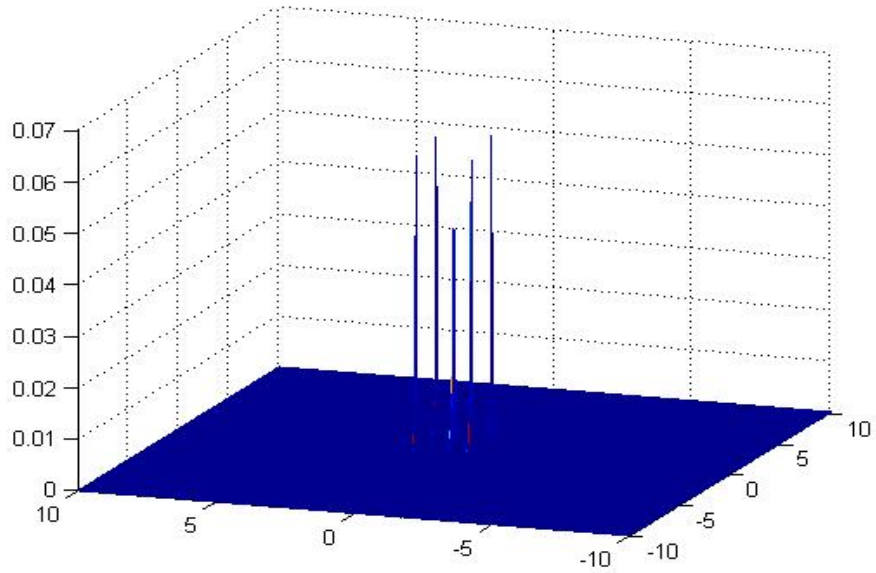
(a)
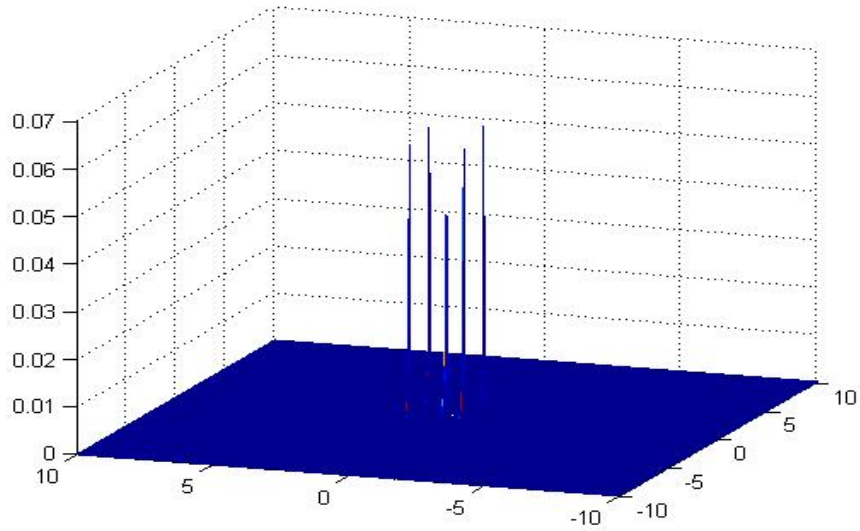
(b)

Figure 15.   Amplitude of field scattered from 5 points using Born (a) and Rytov (b) approximations

Figure 15 shows 5 scattering points applying the Born and Rytov approximations at $z = 2m$. We will add Gaussian noise to this data and use Tikhonov regularization, truncated SVD methods, and the L-curve method discussed in chapter 2. All MATLAB codes are presented in Appendix D.

C.   SIMULATION RESULTS

To compare the Born and Rytov approximations, first we simulate with equation (6.9) and equation (6.35) separately. We get Figure 15 (a) from the Born approximation and Figure 15 (b) from the Rytov approximation. These two figures look very similar, and they localize the scatterers equally well. But the strength of each peak differs by 1.2% in both figures. The difference is formed by subtracting equation (6.35) from equation (6.9) and simulating again. Figure 16 shows us the differences between them. The differences of each peak are approximately 0.16%, and both approximations perform equally well.

D.   SIGNAL TO NOISE RATIO

For the simulation of measuring a scattered electric field, we have to add noise to the original signal from the Rytov approximation, since signals are corrupted by noise in nature. We will use the Gaussian noise that is commonly used as an additive noise model in physics. Since the Signal to Noise Ratio (SNR) is defined as the ratio of signal power to noise power, we calculate the SNR by taking the ratio of the sum of the signal and the Gaussian noise in the frequency domain. Furthermore we find the minimum SNR to recognize the image of objects by increasing a noise factor.
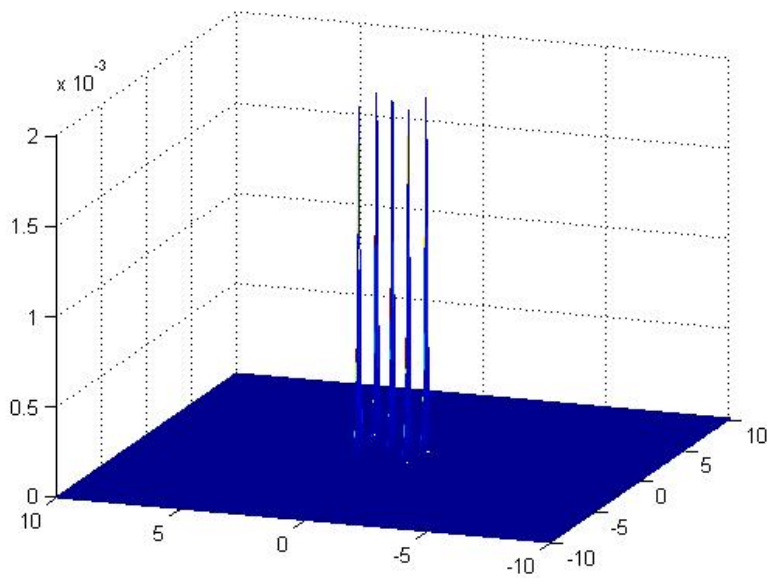
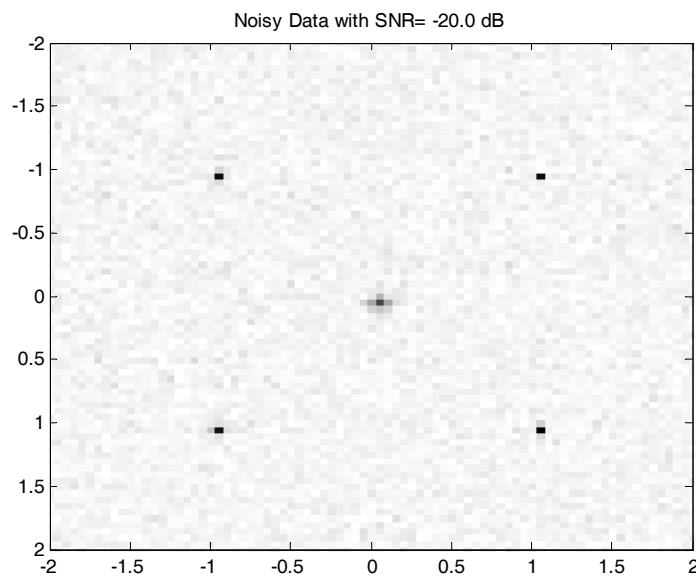Figure 16.   Differences between Born and Rytov approximations

Figure 17.   Scattering points with Gaussian noise SNR=-20dB

E.   TIKHONOV REGULARIZATION

Figure 17 shows the scattered signals with noise. We use Tikhonov regularization to mitigate these noise effects. During this process there is a trade-off between the regularized output and the original data. In order to optimize the trade-off, we have to choose the best regularization parameters. To find the regularization parameters we will use L-curve method. The L-curve method is based on a log-log plot of the norm of the residual versus the solution for a range of values of regularization parameters [14]. The common expression of the Tikhonov regularization is

$$F_\alpha = \|AX - b\|_2^2 + \alpha \|X\|_2^2 \qquad (7.8)$$

where $\|AX - b\|_2^2$ is a residual norm, $\|X\|_2^2$ is a regularized solution, and α is the regularization parameter. The "horizontal" part of the L-curve is dominated by regularization errors that occur from over-smoothing and the "vertical" part is dominated by perturbation errors that occur from under-smoothing. Hence, we choose our optimal solution as the one at the corner of the L-curve in Figure 18(b). So a particular regularization parameter is $\alpha = 4.6$. Using this parameter we can get a good recovered image in Figure 19. However, Figure 20 shows us that if we use regularization parameter smaller than the optimal one, we will get an unstable image.

(a)   (b)
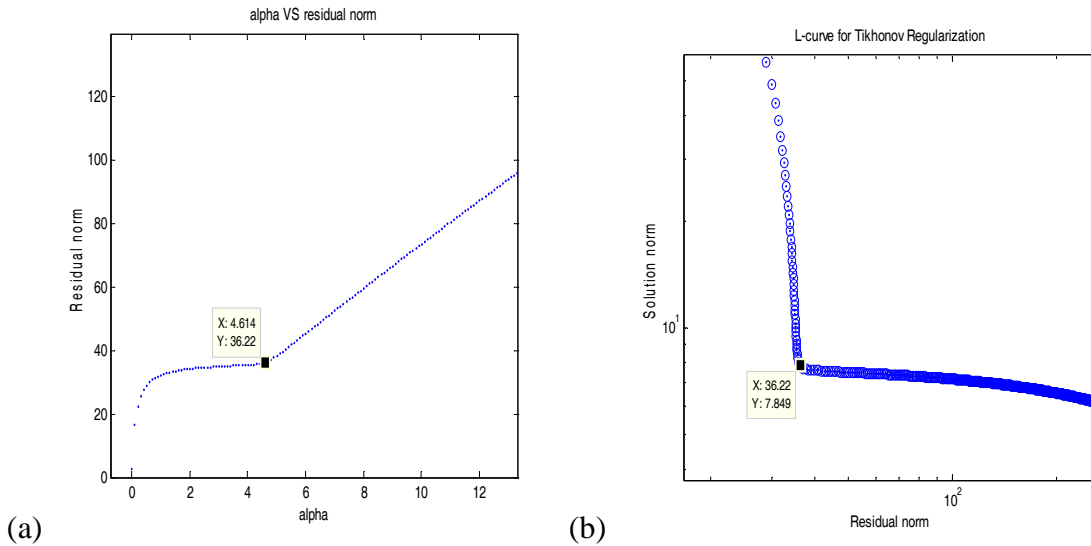
Figure 18.   Regularization parameter (a) and L-curve (b)

58
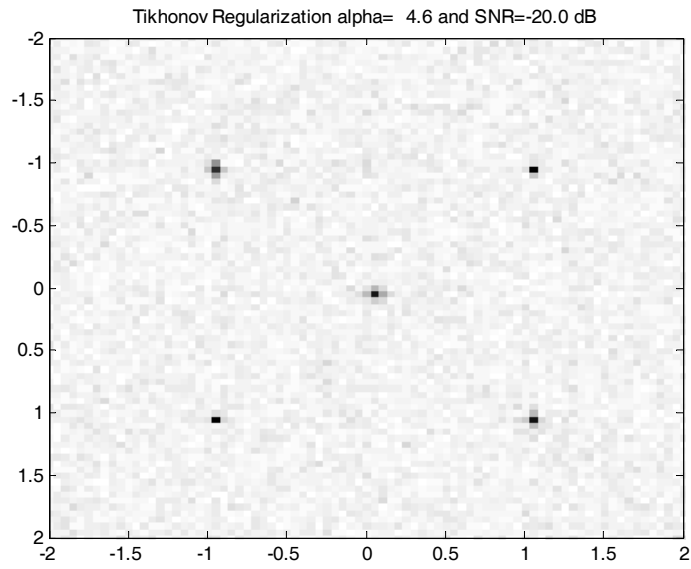
Figure 19.   Tikhonov Regularization α =4.6 at SNR=-20dB
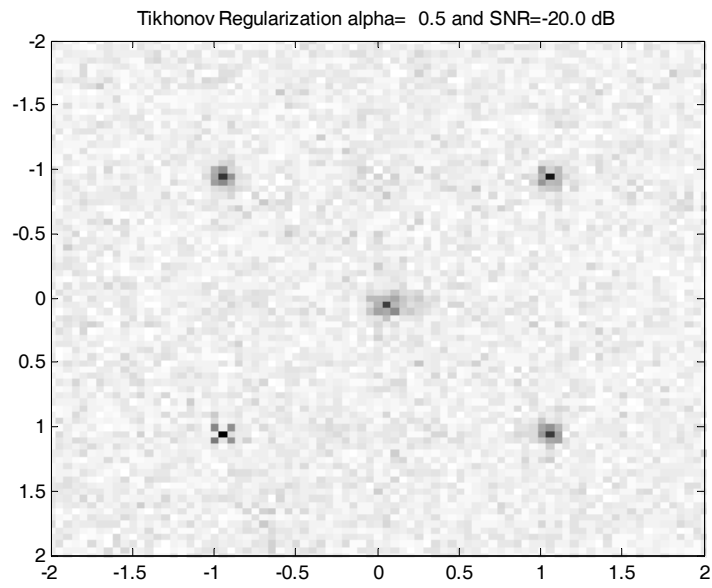
Figure 20.   Tikhonov Regularization α =0.5 at SNR=-20dB

F.   TRUNCATED SVD

Since the operator *A* of TWI has large singular values, we can apply the truncated SVD method. Using the singular value spectrum plot in Figure 21, we can find values $\mathcal{K} = 0.34$ and , $\mathcal{K} = 0.10$ where the singular values change rapidly, and truncate with these values. Figure 22 is obtained by truncating $\mathcal{K} = 0.34$,and Figure 23 is obtained by truncating $\mathcal{K} = 0.10$. These two figures are good examples of optimal truncation parameters.

On the contrary, Figure 24, obtained at $\mathcal{K} = 100$, shows that a too-large $\mathcal{K}$ affects the accuracy of estimation.
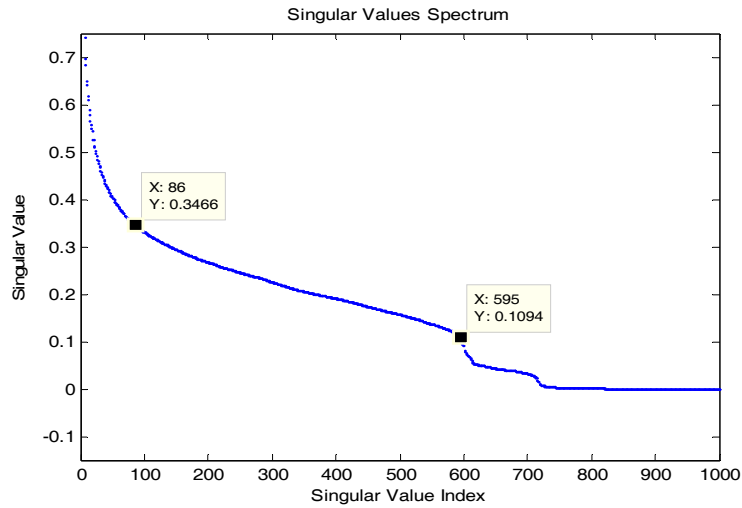
Figure 21.   Singular value spectrum of transfer operator

Figure 22.   TSVD K =0.34 at SNR=-20dB
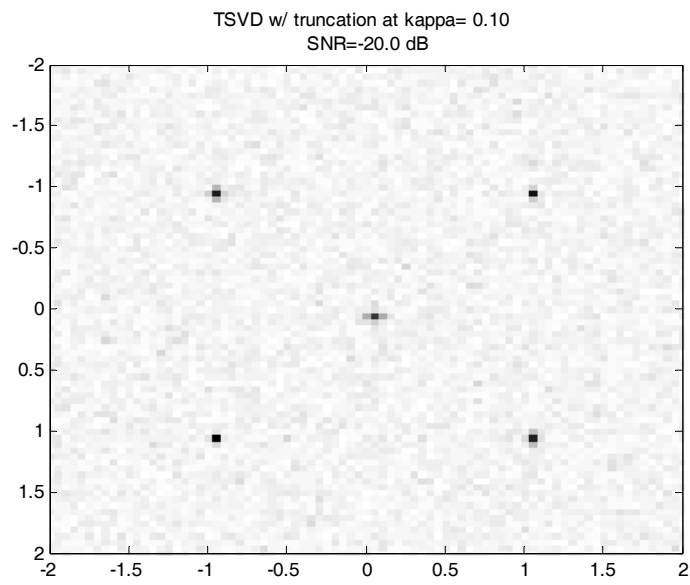
Figure 23.   TSVD K =0.10 at SNR=-20dB
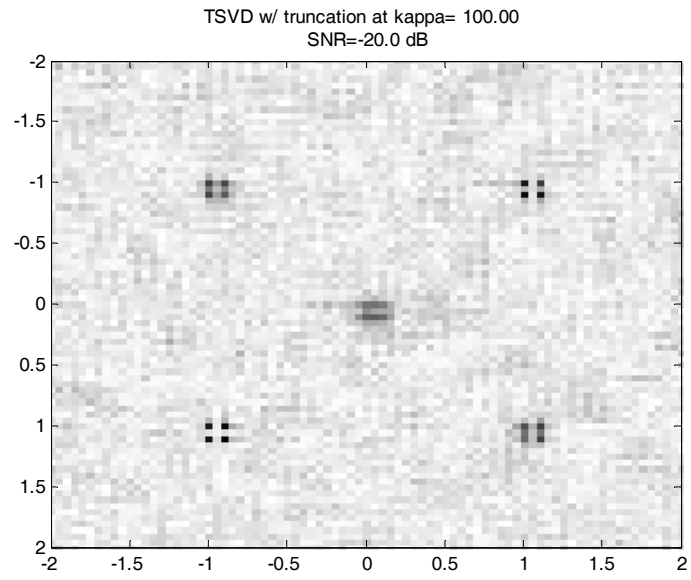
Figure 24.   TSVD Κ =100 at SNR=-20dB

THIS PAGE INTENTIONALLY LEFT BLANK

VIII. CONCLUSION

In recent years, a variety of techniques for THz imaging have been developed for the detection of weapons, explosives, and drugs at security check points and for the detection of illegal immigrants at the border. This thesis is a review of some of this work. We think our model may be useful for military and security officers to detect enemies hiding in a room or behind a wall.

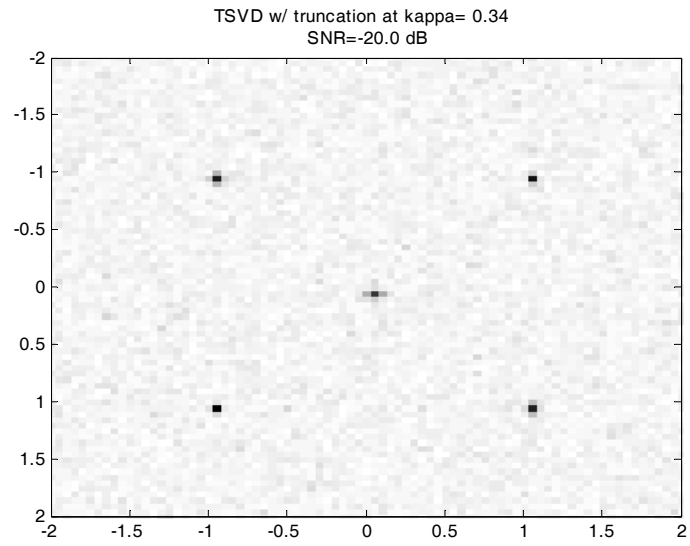In this thesis we have applied the Born and Rytov approximations to the problem of imaging from scattered field measurements. Also we examined the Tikhonov regularization parameter selection with the L-curve method. The simulation result obtained by the Rytov approximation has been compared to one yielded by the Born approximation. The difference between them is insignificant. Therefore the Rytov approximation appears to be no better than the Born approximation. It would be useful to apply this simulation to real data in the future. In general, the Rytov approximation is more accurate than the Born approximation especially, at higher frequencies [24].

Further modeling efforts are also required. We have assumed the medium (wall) is linear, nonmagnetic, and nonconductive. But in reality, wall materials are not exactly like this. Some materials are nonlinear, magnetic, and conductive. So for this case, the wave equation has to be adjusted to derive a new Green's function to fit this model, and we have to apply vector theory instead of scalar theory to the wave equation.

For more accurate image reconstruction, we also need to consider dispersive effects of different kinds of walls and have to include multiple scattering effects to the Lippman-Schwinger equation.

THIS PAGE INTENTIONALLY LEFT BLANK

APPENDIX A. SINGULAR VALUE DECOMPOSITION

Let $K \in \square^{M \times N}$ is a linear operator which maps vectors $f \in \square^{N}$ to vectors $d \in \square^{M}$. We will consider two symmetric matrices $K^{T}K(N \times N)$ and $KK^{T}(M \times M)$. Since these matrices are square and symmetric, we can get eigenvectors and eigenvalues of each. If λ_{i} is the eigenvalue and f_{i} is the eigenvector of $K^{T}K$.

The eigen equation for $K^{T}K$ is

$$K^{T}Kf_{i} = \lambda_{i}f_{i} \tag{A.1}$$

Applying the same method, we get the eigen equation for KK^{T}

$$KK^{T}d_{i} = \gamma_{i}d_{i} \tag{A.2}$$

If we take the eigenvector f_{i} of $K^{T}K$, and the eigenvalue $\lambda_{i} \neq 0$, then we get vector $Kf_{i} \neq 0$, this can be proved here

$$(KK^{T})Kf_{i} = K(K^{T}K)f_{i} = K(\lambda_{i})f_{i} = \lambda_{i}(Kf_{i}) \tag{A.3}$$

Hence Kf_{i} is an eigenvector of KK^{T} and each eingenvalue $\lambda_{i} \neq 0$ of $K^{T}K$ must be an eigenvalue of KK^{T}. Similarly, this is also true each eigenvalue $\gamma_{i} \neq 0$ of KK^{T} must be an eigenvalue of $K^{T}K$.

If there are r non-zero eigenvalues of $K^{T}K$ (or KK^{T}), where $r \leq m$ and $r \leq n$, we can express it like this

$$\lambda_{1} = \gamma_{1}$$
$$\lambda_{2} = \gamma_{2}$$
$$\vdots$$
$$\lambda_{r} = \gamma_{r}$$
$$\lambda_{r+1} = 0 \quad \gamma_{r+1} = 0$$
$$\vdots \qquad \vdots$$
$$\lambda_{n} = 0 \qquad \gamma_{m} = 0$$

Therefore the linear equation is expressed

$$f = K^T d \qquad d = Kf \tag{A.4}$$

Then we normalize eigenvectors

$$f = \frac{K^T d}{\|K^T d\|} \quad d = \frac{Kf}{\|Kf\|} \tag{A.5}$$

The singular values σ_k of K are defined by

$$\|Kf_k\| = \|K^T d_k\| = \sigma_k = \sqrt{\lambda_k} = \sqrt{\gamma_k} \tag{A.6}$$

So equation (A.5) becomes for $K \leq M, N$.

$$K^T d_k = \sigma_k f_k , \quad Kf_k = \sigma_k d_k \tag{A.7}$$

but for $K > M, N$, the equation becomes

$$Kf_k = 0 \qquad for \ k = r+1, \cdots N \tag{A.8}$$

$$K^T d_k = 0 \quad for \ k = r+1, \cdots M \tag{A.9}$$

On equation (A.7), we take $Kf_k = \sigma_k d_k$ and multiply by f_k^T on both sides. Then it becomes

$$K^T = \sum_{i=1}^{r} \sigma_i f_i d_i^T \tag{A.10}$$

And the other one in equation (A.7) becomes

$$K = \sum_{i=1}^{r} \sigma_i d_i f_i^T \tag{A.11}$$

We can write equation (A.11) in matrix form as

$$K = \begin{bmatrix} \vdots & \vdots & \vdots \\ d_1 & d_2 & \cdots \\ \vdots & \vdots & \vdots \end{bmatrix} \begin{bmatrix} \sigma_1 & 0 & 0 \\ 0 & \sigma_2 & 0 \\ 0 & 0 & \ddots \end{bmatrix} \begin{bmatrix} \cdots & f_1 & \cdots \\ \cdots & f_2 & \cdots \\ \vdots & \vdots & \vdots \end{bmatrix} \tag{A.12}$$

or $K = DUF^T$

where, U is a diagonal matrix of the singular values, and D and F consist of the eigenvectors corresponding to those singular values. f and d are the orthonomal vectors and called right singular vectors and left singular vectors respectively.

66

We can make the inverse of K as

$$K^{-1} = (DUF^T)^{-1} \qquad (A.13)$$

We know F^T and D are orthogonal matrices, because they are composed of eigenvectors which are orthogonal. Equation (A.13) becomes

$$K^{-1} = (F^T)^{-1} U^{-1} D^{-1} \qquad (A.14)$$

$$K^{-1} = F U^{-1} D^T \qquad (A.15)$$

U^{-1} is a diagonal matrix composed of $\dfrac{1}{\sigma}$. Since singular values of K are in the order of

$$\sigma_1 \geq \sigma_2 \geq \cdots \geq \sigma_r > 0 \qquad (A.16)$$

elements in a matrix U^{-1} will increase infinitely [10]. Hence, the norm of inverse mapping K^{-1} also will increase. This is why we need a regularization method for the inverse imaging.

THIS PAGE INTENTIONALLY LEFT BLANK

APPENDIX B. GREEN'S FUNCTION

Green's function satisfies a wave equation driven by a point source.

$$(\nabla^2 + k^2)\psi(r) = S(r) \tag{B.1}$$

To obtain a solution to wave equation need to seek the Green's function that is the solution to the following equation.

$$(\nabla^2 + k^2)G(r, r') = -\delta(r - r') \tag{B.2}$$

If we let arbitrary source $S(r)$

$$S(r) = \int S(r')\delta(r - r')dr' \tag{B.3}$$

Then we can write

$$\psi(r) = -\int G(r, r')S(r')dr' \tag{B.4}$$

To find a solution of equation (B.2), solve it in spherical coordinates with the origin at r'

$$(\nabla^2 + k^2)G(r) = -\delta(r) = -\delta(x)\delta(y)\delta(z) \tag{B.5}$$

Due to the spherical symmetry of a point source, $G(r)$ is also spherical symmetric.

In spherical coordinates equation (B.2) becomes as

$$\frac{1}{r}\frac{d^2}{dr^2}(rG) + k^2G = -\delta(r) \tag{B.6}$$

Everywhere, except at $r = 0$, the equation is the same as the homogeneous equation

$$\frac{d^2}{dr^2}(rG) + k^2(rG) = 0 \tag{B.7}$$

So the solution is shown below

$$G(r) = A\frac{e^{ikr}}{r} + B\frac{e^{-ikr}}{r} \tag{B.8}$$

Since sources are absent at infinity, only an outgoing solution can exist.

$$G(r) = A\frac{e^{ikr}}{r} \tag{B.9}$$

To find the constant A, substitute equation (B.9) into equation (B.2) and integrate equation (B.2) over a small volume.

$$\int_{\square V} \nabla \cdot \nabla \frac{Ae^{ikr}}{r} + \int_{\square V} k^2 \frac{Ae^{ikr}}{r} = -1 \tag{B.10}$$

Since $dV = 4\pi r^2 dr$, the second integral vanishes and the first integral is converted into a surface integral using Gauss' Theorem

$$\lim_{r \to 0} 4\pi r^2 \frac{d}{dr} \frac{Ae^{ikr}}{r} = -1 \tag{B.11}$$

Finally we get $A = \dfrac{1}{4\pi}$

Therefore, the Greens' function G is

$$G(r - r') = \frac{e^{ik|r-r'|}}{4\pi |r - r'|} \tag{B.12}$$

Consequently, the final solution to equation (B.1) is

$$\psi(r) = -\int_V \frac{e^{ik|r-r'|}}{4\pi |r - r'|} S(r') dr' \tag{B.13}$$

APPENDIX C. FOURIER TRANSFORM IN 2-D

When dealing with both linear and nonlinear systems, it is useful to break down a complicated input into more simple inputs. This process is well known as the Fourier Transform. The Fourier Transform of a complex-valued function g of two independent variables x and y is defined by

$$\mathcal{F}\{g\} = \int\int_{-\infty}^{\infty} g(x,y)e^{-i2\pi(v_x x + v_y y)}dxdy \tag{C.1}$$

Similarly, the Inverse Fourier Transform of a $G(v_x, v_y)$ is defined as

$$\mathcal{F}^{-1}\{G\} = \int\int_{-\infty}^{\infty} G(v_x, v_y)e^{i2\pi(v_x x + v_y y)}dv_x dv_y \tag{C.2}$$

But all functions cannot be transformed from the spatial domain into Fourier domain. In order to be transformed, the function should satisfy "existence conditions" [20].

1. 'g' must be absolutely integrable over the infinite (x, y) plane.

2. 'g' must have a finite number of discontinuities and a finite number of maxima and minima in any finite rectangle.

3. 'g' must have no infinite discontinuities.

There are a few useful properties of the Fourier Transform. These will provide the basic idea for the manipulation of the Fourier Transforms and can save time solving Fourier problems.

1. Linear Theorem :

$$\mathcal{F}(\alpha g + \beta k) = \alpha\mathcal{F}(g) + \beta\mathcal{F}(k) \tag{C.3}$$

2. Similarity Theorem

If $\mathcal{F}\{g(x,y)\} = G(v_x, v_y)$, then $\mathcal{F}\{g(ax, by)\} = \dfrac{1}{|ab|}G(\dfrac{v_x}{a}, \dfrac{v_y}{b})$ \hfill (C.4)

3.   **Shift Theorem :**

If $\mathcal{F}\{g(x,y)\} = G(v_x, v_y)$, then $\mathcal{F}\{g(x-a, y-b)\} = G(v_x, v_y)e^{-i2\pi(v_x a + v_y b)}$ (C.5)

4.   **Parseval's Theorem :**

If $\mathcal{F}\{g(x,y)\} = G(v_x, v_y)$, then $\int\limits_{-\infty}^{\infty}\int |g(x,y)|^2 dxdy = \int\limits_{-\infty}^{\infty}\int |G(v_x, v_y)|^2 dv_x dv_y$ (C.6)

5.   **Convolution Theorem :**

If $\mathcal{F}\{g(x,y)\} = G(v_x, v_y)$ and $\mathcal{F}\{K(x,y)\} = KG(v_x, v_y)$, then

$$\mathcal{F}\left\{\int\limits_{-\infty}^{\infty}\int g(a,b)K(x-a, y-b)dadb\right\} = G(v_x, v_y)K(v_x, v_y)$$ (C.7)

6.   **Autocorrelation Theorem**

If $\mathcal{F}\{g(x,y)\} = G(v_x, v_y)$, then

$$\mathcal{F}\left\{\int\limits_{-\infty}^{\infty}\int g(a,b)g*(a-x, b-y)dadb\right\} = |G(v_x, v_y)|^2$$ (C.8)

similarly, $\mathcal{F}\left\{|g(x,y)|^2\right\} = \int\limits_{-\infty}^{\infty}\int |G(a,b)^2|G*(a-v_x, b-v_y)dadb$ (C.9)

APPENDIX D. MATLAB CODES

%%%%%%%%%%% Matlab code for material reflection %%%%%%%%%%%%%

```matlab
clear;
% Calculating the Reflection for plane waves in various surface
% Equations used from Chapter 5
% Creating various index of refraction for different materials
% Polystyrene foam, Quartz, Glass
nm=[1.01 1.5 1.8];
% Lophira alata(wood), Tile, Sand
% nm=[1.49 1.6 1.67];
% Skin, Body fluid
% nm=[1.4 3.9];

% Thickness of the material
L=0.5;
c=3.0e8;     % Speed of light

figure(1)

  nu=linspace(1e11,5e12,100);
  k=2*pi*nu./c;
  num=(1-nm(1)^2)+(nm(1)^2-1)*exp(i*2*k*L*nm(1));
  den=(nm(1)+1)^2-((nm(1)-1)^2)*exp(i*2*k*L*nm(1));
  r=num./den;
  R=r.*conj(r);
  hold on
  plot(nu,R,'-');
  gtext(sprintf('n=%2.2f',nm(1)));

  num=(1-nm(2)^2)+(nm(2)^2-1)*exp(i*2*k*L*nm(2));
  den=(nm(2)+1)^2-((nm(2)-1)^2)*exp(i*2*k*L*nm(2));
  r=num./den;
  R=r.*conj(r);
  hold on
  plot(nu,R,'-.');
  gtext(sprintf('n=%2.2f',nm(2)));

  num=(1-nm(3)^2)+(nm(3)^2-1)*exp(i*2*k*L*nm(3));
  den=(nm(3)+1)^2-((nm(3)-1)^2)*exp(i*2*k*L*nm(3));
  r=num./den;
  R=r.*conj(r);
  hold on
```

```
    plot(nu,R,':');
    gtext(sprintf('n=%2.2f',nm(3)));

hold off
xlabel('frequency (\nu) Hz');
ylabel('Reflection');
title('Frequency vs Reflection from the dielectric')
gtext(sprintf('L = %1.2f',L));

%%%%%%%%%% Matlab code for Born and Rytov approximations %%%%%%%%

clear;
%parameters
nu=940e9;                % Frequency of the wave propagation.
lambda=3.0e8/nu;         % In terms of wave length.
%k=2*pi/lambda;           % Magnitude of the propagation vector.
k=3000;
n=1.67;                  % Material index of refraction.
L=0.5;                   % Thickness of the wall.
Z=2;                     % Measurement plane at Z=constant. Adjust accordingly
                         % depending on position of the receiver.
A=1;                     % Amplitude of the incident plane wave.
signal=0;
noise=0;

% Defining Coordinate Systems in the spatial frequency domain.
ii=10;                   % Spatial frequencies for meshgrid input.
fb=ii;                   % Frequency band.
%fn=fb;
fn=2*fb;                 % Nyquist rate.
j=1/fn;                  % Separation must be at least this distance to prevent aliasing.
[fx,fy]=meshgrid(-ii:j:ii,-ii:j:ii);         % Creating coordinate system.

% Defining the Green's function.
x0=0; y0=0; z0=-3;                 % Set this position accordingly to the problem.
N=sqrt(k^2-(2*pi*fx).^2-(2*pi*fy).^2);        % Look in chapter 4 for reference.
Nm=sqrt((n*k)^2-(2*pi*fx).^2-(2*pi*fy).^2);   % Look in chapter 4 for reference.
num=4*N.*Nm*exp(-i*N*L);                      % Numerator of the equation.
den=(Nm+N).^2.*exp(-i*Nm*L)-(Nm-N).^2.*exp(i*Nm*L);      % Denominator of the
equation.
% Required terms for taking Fourier transform
A0=exp(-i*2*pi*fx*x0).*exp(-i*2*pi*fy*y0);
G=(num./den).*exp(i*N*Z).*exp(i*N*z0)./(2*N).*A0;  % Transmission Green's function.

%% Synthetic Data Generation
```

```
% Transmittance for a plane wave through a given media
t=4*n*exp(-i*k*L)./((n+1)^2*exp(-i*n*k*L)-(n-1)^2*exp(i*n*k*L));

% scattering Points in the spatial frequency domain.
x1=-1;  y1=-1;  z1=-1;
x2=-1;  y2=1;   z2=-3;
x3=0;   y3=0;   z3=-5;
x4=1;   y4=1;   z4=-1.3;
x5=1;   y5=-1;  z5=-2.2;

% Incident field after the penetration of the media.
E1=t*A*exp(-i*k*z1);
E2=t*A*exp(-i*k*z2);
E3=t*A*exp(-i*k*z3);
E4=t*A*exp(-i*k*z4);
E5=t*A*exp(-i*k*z5);

% Position of the scatter points in frequency domain for the given
% measurement plane at Z=constant
% Since the scatter points are in terms of dirac delta functions,
% the field measurement would become the summation of the Green's function
% and the incident wave after performing the Rytov Approximation
G1=(num./den).*exp(i*N*Z).*exp(i*N*z1)./(2*N);
G2=(num./den).*exp(i*N*Z).*exp(i*N*z2)./(2*N);
G3=(num./den).*exp(i*N*Z).*exp(i*N*z3)./(2*N);
G4=(num./den).*exp(i*N*Z).*exp(i*N*z4)./(2*N);
G5=(num./den).*exp(i*N*Z).*exp(i*N*z5)./(2*N);

% Required terms for taking Fourier transform
A1=exp(-i*2*pi*fx*x1).*exp(-i*2*pi*fy*y1);
A2=exp(-i*2*pi*fx*x2).*exp(-i*2*pi*fy*y2);
A3=exp(-i*2*pi*fx*x3).*exp(-i*2*pi*fy*y3);
A4=exp(-i*2*pi*fx*x4).*exp(-i*2*pi*fy*y4);
A5=exp(-i*2*pi*fx*x5).*exp(-i*2*pi*fy*y5);

%% Generating Data with Born approximation
D=(E1.*G1.*A1+E2.*G2.*A2+E3.*G3.*A3+E4.*G4.*A4+E5.*G5.*A5);

%% Generating Data with Rytov approximation
DD=E1.*(exp(G1.*A1)-1)+E2.*(exp(G2.*A2)-1)+E3.*(exp(G3.*A3)-
1)+E4.*(exp(G4.*A4)-1)+E5.*(exp(G5.*A5)-1);

%% Generating differences by subtracting Born with Rytov
% Generating Data with Born
```

```matlab
B=(E1.*G1+E2.*G2+E3.*G3+E4.*G4+E5.*G5);

% Generating Data with Rytov
R=E1.*(exp(G1)-1)+E2.*(exp(G2)-1)+E3.*(exp(G3)-1)+E4.*(exp(G4)-
1)+E5.*(exp(G5)-1);

Ext=(B-R).*(A1+A2+A3+A4+A5);        % Data with extra terms

% Setting matrix dimension
[MM,NN]=size(D);
D=D(1:MM,1:NN);         % Change matrix dimension if warranted.

% Converting bin numbers to real axis numbers in spatial domain(meters).
% Range has to be up to Nyquist frequency.
ax=linspace(-fn/2,fn/2,length(D));
%% End of Data Generation

figure(1)
d1=ifft2(D);          % Data in the spatial domain.
d1=ifftshift(d1);

mesh(ax,ax,abs(d1));    % Amplitude of field scattered from 5 points using Born
view(-70,20)

figure(2)
d2=ifft2(DD);           % Data in the spatial domain.
d2=ifftshift(d2);

mesh(ax,ax,abs(d2));    % Amplitude of field scattered from 5 points using Rtov
view(-70,20)

figure(3)
d3=ifft2(Ext);          % Data in the spatial domain.
d3=ifftshift(d3);

mesh(ax,ax,abs(d3));    % Differences between Born and Rytov approximations
view(-70,20)

%%%%%%%%%% Matlab code for regularization mathods %%%%%%%%%%%

clear;
%parameters
nu=940e9;          % Frequency of the wave propagation.
lambda=3.0e8/nu;      % In terms of wave length.
%k=2*pi/lambda;        % Magnitude of the propagation vector.
```

```
k=3000;
n=1.67;                         % Material index of refraction.
L=0.5;                          % Thickness of the wall.
Z=2;                            % Measurement plane at Z=constant. Adjust accordingly
                                % depending on position of the receiver.
A=1;                            % Amplitude of the incident plane wave.
signal=0;
noise=0;

% Defining Coordinate Systems in the spatial frequency domain.
ii=10;                          % Spatial frequencies for meshgrid input.
fb=ii;                          % Frequency band.
fn=2*fb;                        % Nyquist rate.
j=1/fn;                         % Separation must be at least this distance to prevent aliasing.
[fx,fy]=meshgrid(-ii:j:ii,-ii:j:ii);            % Creating coordinate system.

% Defining the Green's function.
x0=0; y0=0; z0=-3;                      % Set this position accordingly to the problem.
N=sqrt(k^2-(2*pi*fx).^2-(2*pi*fy).^2);          % Look in chapter 4 for reference.
Nm=sqrt((n*k)^2-(2*pi*fx).^2-(2*pi*fy).^2);     % Look in chapter 4 for reference.
num=4*N.*Nm*exp(-i*N*L);                % Numerator of the equation.
den=(Nm+N).^2.*exp(-i*Nm*L)-(Nm-N).^2.*exp(i*Nm*L);     % Denominator of the
equation.

% Required terms for taking Fourier transform
A0=exp(-i*2*pi*fx*x0).*exp(-i*2*pi*fy*y0);
G=(num./den).*exp(i*N*Z).*exp(i*N*z0)./(2*N).*A0;  % Transmission Green's function.

% Synthetic Data Generation
% Transmittance for a plane wave through a given media
t=4*n*exp(-i*k*L)./((n+1)^2*exp(-i*n*k*L)-(n-1)^2*exp(i*n*k*L));

% scattering Points in the spatial frequency domain.
x1=-1; y1=-1; z1=-1;
x2=-1; y2=1; z2=-3;
x3=0; y3=0; z3=-5;
x4=1; y4=1; z4=-1.3;
x5=1; y5=-1; z5=-2.2;

% Incident field after the penetration of the media.
E1=t*A*exp(-i*k*z1);
E2=t*A*exp(-i*k*z2);
E3=t*A*exp(-i*k*z3);
E4=t*A*exp(-i*k*z4);
E5=t*A*exp(-i*k*z5);
```

% Position of the scatter points in frequency domain for the given
% measurement plane at Z=constant
% Since the scatter points are in terms of dirac delta functions,
% the field measurement would become the summation of the Green's function
% and the incident wave after performing the Rytov Approximation
G1=(num./den).*exp(i*N*Z).*exp(i*N*z1)./(2*N);
G2=(num./den).*exp(i*N*Z).*exp(i*N*z2)./(2*N);
G3=(num./den).*exp(i*N*Z).*exp(i*N*z3)./(2*N);
G4=(num./den).*exp(i*N*Z).*exp(i*N*z4)./(2*N);
G5=(num./den).*exp(i*N*Z).*exp(i*N*z5)./(2*N);

% Required terms for taking Fourier transform
A1=exp(-i*2*pi*fx*x1).*exp(-i*2*pi*fy*y1);
A2=exp(-i*2*pi*fx*x2).*exp(-i*2*pi*fy*y2);
A3=exp(-i*2*pi*fx*x3).*exp(-i*2*pi*fy*y3);
A4=exp(-i*2*pi*fx*x4).*exp(-i*2*pi*fy*y4);
A5=exp(-i*2*pi*fx*x5).*exp(-i*2*pi*fy*y5);

% Generating Data
D=E1.*(exp(G1.*A1)-1)+E2.*(exp(G2.*A2)-1)+E3.*(exp(G3.*A3)-
1)+E4.*(exp(G4.*A4)-1)+E5.*(exp(G5.*A5)-1);

% Setting matrix dimension
[MM,NN]=size(D);
D=D(1:MM,1:NN);   % Change matrix dimension if warranted.

% Converting bin numbers to real axis numbers in spatial domain(meters).
% Range has to be up to Nyquist frequency.
ax=linspace(-fn/2,fn/2,length(D));
n=(randn(MM,NN))+i*(randn(MM,NN));   % noise in complex values in the frequency
domain

% set the signal to noise in dB
SNR=-20;
S=abs(D.*conj(D));
NO=abs(n.*conj(n));
signal=sum(sum(S));
noise=sum(sum(NO));
factor=sqrt((signal/noise)*10^(-SNR/10));
n=n*factor;
d=D+n;   % data with noise in the frequency domain
% End of (noisy) Data Generation

figure(2)   % Data corrupted with noise in spatial domain.

78

```matlab
d1=ifft2(d);                              % Data in the spatial domain.
d1=ifftshift(d1);

imagesc(ax,ax,abs(d1));
colormap (1-gray);
%grid on
axis([-2 2 -2 2])
title(sprintf('Noisy Data with SNR= %3.1f dB',SNR))

% Tikhonov Regularization
[u,s,v]=svd(G);
alpha=4.6;                                % Regularization parameter
Reg=inv(alpha*eye(size(G'*G))+G'*G)*G';

figure(3)
dd=Reg.*d;
dd1=ifft2(dd);                            % Data in the spatial domain
dd1=ifftshift(dd1);
imagesc(ax,ax,abs(dd1));
colormap (1-gray);
%grid on
axis([-2 2 -2 2])
title(sprintf('Tikhonov Regularization alpha= %4.1f and SNR=%3.1f dB',alpha,SNR))

% Truncated SVD Method
kappa=0.34;                               % Parameter for truncation of singular values
[u,s,v]=svd(G);

% inverse of the singular value matrix
sinvlu=zeros(NN,MM);
for j=1:rank(s)
   if 1/s(j,j) < kappa
      sinvlu(j,j)=1/s(j,j);
   else
      sinvlu(j,j)=0;
   end
end

td=(v*sinvlu*u').*d;
TD=ifft2(td);                             % Data in the spatial domain
TD=ifftshift(TD);

figure(4)
imagesc(ax,ax,abs(TD));
colormap (1-gray);
```

79

```matlab
axis([-2 2 -2 2])
title(sprintf('TSVD w/ truncation at kappa= %3.2f \n SNR=%3.1f dB',kappa,SNR))

%%%%%%%%%%%% Matlab code for L-curve plot %%%%%%%%%%%%%

clear;
%parameters
nu=940e9;                              % Frequency of the wave propagation.
lambda=3.0e8/nu;                       % In terms of wave length.
%k=2*pi/lambda;                         % Magnitude of the propagation vector.
k=3000;
n=1.67;                                % Material index of refraction.
L=0.5;                                  % Thickness of the wall.
Z=2;                                    % Measurement plane at Z=constant. Adjust accordingly
                                        % depending on position of the receiver.
A=1;                                    % Amplitude of the incident plane wave.
signal=0;
noise=0;

% Defining Coordinate Systems in the spatial frequency domain.
ii=10;                  % Spatial frequencies for meshgrid input.
fb=ii;                  % Frequency band.
fn=2*fb;                % Nyquist rate.
j=1/fn;                 % Separation must be at least this distance to prevent aliasing.
[fx,fy]=meshgrid(-ii:j:ii,-ii:j:ii);                        % Creating coordinate system.

% Defining the Green's function.
x0=0; y0=0; z0=-3;                             % Set this position accordingly to the problem.
N=sqrt(k^2-(2*pi*fx).^2-(2*pi*fy).^2);             % Look in chapter 4 for reference.
Nm=sqrt((n*k)^2-(2*pi*fx).^2-(2*pi*fy).^2);          % Look in chapter 4 for reference.
num=4*N.*Nm*exp(-i*N*L);                      % Numerator of the equation.
den=(Nm+N).^2.*exp(-i*Nm*L)-(Nm-N).^2.*exp(i*Nm*L);       % Denominator of the
equation.

% Required terms for taking Fourier transform
A0=exp(-i*2*pi*fx*x0).*exp(-i*2*pi*fy*y0);

% Synthetic Data Generation
% Transmittance for a plane wave through a given media
t=4*n*exp(-i*k*L)./((n+1)^2*exp(-i*n*k*L)-(n-1)^2*exp(i*n*k*L));

% scattering Points in the spatial frequency domain.
x1=-1; y1=-1; z1=-1;
x2=-1; y2=1; z2=-3;
x3=0; y3=0; z3=-5;
```

```
x4=1;  y4=1;  z4=-1.3;
x5=1;  y5=-1;  z5=-2.2;

% Incident field after the penetration of the media.
E1=t*A*exp(-i*k*z1);
E2=t*A*exp(-i*k*z2);
E3=t*A*exp(-i*k*z3);
E4=t*A*exp(-i*k*z4);
E5=t*A*exp(-i*k*z5);

% Position of the scatter points in frequency domain for the given
% measurement plane at Z=constant
% Since the scatter points are in terms of dirac delta functions,
% the field measurement would become the summation of the Green's function
% and the incident wave after performing the Rytov Approximation
G1=(num./den).*exp(i*N*Z).*exp(i*N*z1)./(2*N);
G2=(num./den).*exp(i*N*Z).*exp(i*N*z2)./(2*N);
G3=(num./den).*exp(i*N*Z).*exp(i*N*z3)./(2*N);
G4=(num./den).*exp(i*N*Z).*exp(i*N*z4)./(2*N);
G5=(num./den).*exp(i*N*Z).*exp(i*N*z5)./(2*N);

% Required terms for taking Fourier transform
A1=exp(-i*2*pi*fx*x1).*exp(-i*2*pi*fy*y1);
A2=exp(-i*2*pi*fx*x2).*exp(-i*2*pi*fy*y2);
A3=exp(-i*2*pi*fx*x3).*exp(-i*2*pi*fy*y3);
A4=exp(-i*2*pi*fx*x4).*exp(-i*2*pi*fy*y4);
A5=exp(-i*2*pi*fx*x5).*exp(-i*2*pi*fy*y5);

G=G1*A1+G2*A2+G3*A3+G4*A4+G5*A5;

% Generating Data
D=E1.*(exp(G1.*A1)-1)+E2.*(exp(G2.*A2)-1)+E3.*(exp(G3.*A3)-
1)+E4.*(exp(G4.*A4)-1)+E5.*(exp(G5.*A5)-1);

% Setting matrix dimension
[MM,NN]=size(D);
D=D(1:MM,1:NN);                          % Change matrix dimension if warranted.

% Converting bin numbers to real axis numbers in spatial domain(meters).
% Range has to be up to Nyquist frequency.
ax=linspace(-fn/2,fn/2,length(D));
no=(randn(MM,NN))+i*(randn(MM,NN));    % noise in complex values in the frequency
domain

% set the signal to noise in dB
```

```
SNR=-20;
S=abs(D.*conj(D));
NO=abs(no.*conj(no));
signal=sum(sum(S));
noise=sum(sum(NO));
factor=sqrt((signal/noise)*10^(-SNR/10));
no=no*factor;
d=D+no;      % data with noise in the frequency domain
% End of (noisy) Data Generation

% Tikhonov Regularization
[u,s,v]=svd(G);

for alpha=linspace(10^-2,10^2,1000)              % Range of Regularization parameters
  Reg=inv(alpha*eye(size(G'*G))+G'*G)*G'*d;    % Regularized solution
  sol=norm(eye(size(G'*G))*Reg);                % Solution norm
  res=norm(G'*G*Reg-G'*d);                      % Residual norm

  figure(3)
  loglog(res,sol,'-o');
  hold on
  title('L-curve for Tikhonov Regularization');
  xlabel('Residual norm');
  ylabel('Solution norm');
  figure(4)
  plot(alpha,res);
  hold on
  title('alpha VS residual norm');
  xlabel('alpha');
  ylabel('Residual norm');

end

title('L-curve for Tikhonov Regularization')
xlabel('Residual norm');
ylabel('Solution norm');
axis([10^-4 10^4 10^0 10^8])
```

LIST OF REFERENCES

[1] Kodo Kawase, "For drug detection and large-scale integrated circuit inspection," Optics and photonics news, October 2004, http://www.nuee.nagoya-u.ac.jp/labs/optlab/kawase/JP/41_h27.pdf .

[2] R. Jennifer Hwu, "Terahertz for military and security application II," Proceedings of SPIE, vol.5411, April 2004.

[3] James William Handley, "Time frequency analysis techniques in terahertz pulsed imaging," Ph.D. dissertation, University of Leeds School of Computing, Leeds, West Yorkshire, UK, December 2003.

[4] R. Jennifer Hwu, "Terahertz for military and security applications," Proceedings of SPIE, vol. 5070, April 2003.

[5] Christopher A. Miles, "Through-the-wall surveillance: New technology for saving lives," //http://www.ojp.usdoj.gov/nij/journals/258/index.html.

[6] C. W. Groetsch, "The theory of Tikhonov regularization for Fredholm equations of the first kind," research notes in mathematics, Pitman Advanced Publishing Program, Boston, London, Melbourne, 1984.

[7] S. Wang and X.-C. Zhang,"Pulsed terahertz tomography," J. Phys. D: Appl. Phys. 37(2004) R1-R36, Center for Terahertz Research, Troy, NY, January 2004.

[8] J. Martyn Chamberlain, "Terahertz spectroscopy and applications II," Proceedings EUROPTO Series, vol. 3828, June 1999.

[9] Borden, Brett, "Radar Imaging of Airborne Targets," Institute of Physics Publishing Bristol and Philadelphia, April 1999.

[10] David S. Watkins, "Fundamentals of Matrix Computations Second Edition," John Wiley & Sons, Inc, New York, NY, 2002.

[11] Dana H. Brooks and Charles A. Dimarzio, "A comparison study of linear reconstruction techniques for diffuse optical tomographic imaging of absorption coefficient," Phys.Med.Biol.45(2000), Printed in the UK, January 2000, http://www.nmr.mgh.harvard.edu/PMI/PDF/Gaudette 2000.pdf.

[12] H. Lauter and H. Liero, "Ill-posed inverse problems and their optimal regularization," Potsdam, Germany, July 1997.

[13] Per Christian Hansen, "Regularization tools," Lyngby, Denmark, March 2008, http://www.imm.dtu.dk/~pch.

[14] "Total variation regularization and L-curve method for the selection of regularization parameter," class notes for ECE 599, The University of Tennessee, TN, Summer 2003.

[15] Albert D. Wheelon, "Electromagnetic Scintillation II. Weak Scattering," Cambridge University, New York, NY, 2003.

[16] Jin Au Kong, " Electromagnetic Wave Theory," Published by John Willey and Sons, Inc., Cambridge, Massachusetts, 1986.

[17] Sophocles J. Orfanidis, "Electromagnetic waves and antennas," ECE Department Rutgers University, http://www.ece.rutgers.edu/orfanidi/ewa/.

[18] David H. Staelin, Ann W. Morgenthaler and Jin Au Kong, "Electromagnetic Waves," Prentice Hall, inc., Englewood Cliffs, New Jersey, 1994.

[19] Jack Vanderlinde, "Classical Electromagnetic Theory Second Edition," Kluwer Academic Publishers, Dordrecht, Boston, London, 2004.

[20] Joseph W. Goodman, "Introduction to Fourier Optics 3rd Edition," Roberts and Company Publishers, Greenwood, Colorado, 2005.

[21] Ajoy Ghatak, "Optics 3rd Edition," The McGraw-Hill companies, 2005.

[22] Weng Cho Chew, "Waves and Fields in Inhomogeneous Media," IEEE, New York, NY, 1995.

[23] James F. Shackelford, "Materials Science for Engineers Fifth Edition," Prentice-Hall, Inc., Upper Saddle River, New Jersey, 2000.

[24] "T-ray diffraction tomography," "Ph.D. dissertation," http://thesis.library.adelaide.edu.au/uploads/approved/adt-SUA20050502.150032/public/09chapter6.pdf.

INITIAL DISTRIBUTION LIST

1. Defense Technical Information Center
   Ft. Belvoir, Virginia

2. Dudley Knox Library
   Naval Postgraduate School
   Monterey, California

3. Professor Brett Borden
   Naval Postgraduate School
   Monterey, CA

4. Professor Gamani Karunasiri
   Naval Postgraduate School
   Monterey, CA